
Article:
Ely, J.C. orcid.org/0000-0003-4007-1500, Clark, C.D. orcid.org/0000-0002-1021-6679, Bradley, S.L. orcid.org/0000-0003-3740-5696 et al. (5 more authors) (2024) Behavioural tendencies of the last British–Irish Ice Sheet revealed by data–model comparison. Journal of Quaternary Science, 39 (6). pp. 839-871. ISSN 0267-8179

https://doi.org/10.1002/jqs.3628

JOURNAL OF QUATERNARY SCIENCE (2024) 1–33 ISSN 0267-8179. DOI: 10.1002/jqs.3628

JQS Journal of Quaternary Science QRA Quaternary Research Association

Behavioural tendencies of the last British–Irish Ice Sheet revealed by data–model comparison

JEREMY C. ELY,[1]* CHRIS D. CLARK,[1] SARAH L. BRADLEY,[1] LAUREN GREGOIRE,[2] NIALL GANDY,[3] ED GASSON,[4] REMY L.J. VENESS[1,3] and ROSIE ARCHER[1]

[1]Department of Geography, University of Sheffield, Sheffield, S10 2TN, UK
[2]School of Earth and Environment, University of Leeds, Leeds, LS2 9JT, UK
[3]Department of the Natural and Built Environment, Sheffield Hallam University, Sheffield, S1 1WB, UK
[4]Department of Earth and Environmental Sciences, University of Exeter, Penryn Campus, Penryn, Cornwall, TR10 9FE, UK

Received 9 February 2024; Revised 8 May 2024; Accepted 14 May 2024

ABSTRACT: Integrating ice-sheet models with empirical data pertaining to palaeo-ice sheets promotes advances in the models used in sea-level predictions and can improve our understanding of past ice-sheet behaviour. The large number of empirical constraints on the last British–Irish Ice Sheet make it ideal for model–data comparison experiments. Here, we present an ensemble of 600 model simulations, which are compared with data on former ice-flow extent, flow geometry and deglaciation timing. Simulations which poorly recreate data were ruled out, allowing us to examine the remaining physically realistic simulations which capture the ice sheets' behavioural tendencies. Our results led to a novel reconstruction of behaviour in the data-poor region of the North Sea, insights into the ice stream, potential ice-shelf and readvance dynamics, and the potential locations of peripheral ice caps. We also propose that the asynchronous behaviour of the British–Irish Ice Sheet is a consequence of the geography of the British Isles and the merging and splitting of different bodies of ice through saddle merger and collapse. Furthermore, persistent model–data mismatches highlight the need for model development, especially regarding the physics of ice–ocean interactions. Thus, this work highlights the power of integrating models and data, a long-held aim of palaeoglaciology. © 2024 The Authors. *Journal of Quaternary Science* Published by John Wiley & Sons Ltd.

KEYWORDS: British–Irish Ice Sheet; glaciology; ice sheet; numerical modelling; palaeoglaciology

Introduction

Reconstructing palaeo-ice sheets enables us to understand the centennial and millennial scale response of ice sheets to climate change (Stokes et al., 2015), which in turn can aid our understanding of glacial processes (e.g. Boulton and Clark, 1990; Kleman and Glasser, 2007; Stokes et al., 2016; Gandy et al., 2019) and inform projections of contemporary ice sheets in our warming world (e.g. DeConto and Pollard, 2016). Though overlap exists (e.g. Tarasov et al., 2012; Gandy et al., 2021), there are broadly two approaches to reconstructing palaeo-ice dynamics. The first, the empirical approach, examines the evidence left behind by palaeo-ice sheets after deglaciation to create reconstructions of past ice-sheet extent, timing and dynamics (e.g. Clark et al., 2012; Hughes et al., 2016; Dalton et al., 2020; Davies et al., 2020). This takes the form of examinations of glacial sediments (e.g. Ó Cofaigh and Dowdeswell, 2001; Evans and Thomson, 2010), geochronological constraints from dated materials (e.g. Dyke, 2004; Small et al., 2017) and mapping of glacial landforms (e.g. Clark et al., 2018). The second, a model-based approach, applies the numerical models used to forecast the fate of contemporary ice sheets to hindcast palaeo-ice sheet behaviour (e.g. Fisher et al., 1985; Tarasov and Peltier, 2004; Hubbard et al., 2009; Patton et al., 2017). Model experiments of palaeo-ice sheets are useful for reconstructing ice dynamics, evaluating model skill, and testing formulations (e.g. Aschwanden et al., 2013; Gandy et al., 2019). Notably, data on relative sea level and uplift is often interrogated by glacio-isostatic modelling to infer past ice loading, though the degree to which realistic ice geometries are incorporated into this modelling varies (e.g. Simpson et al., 2009; Bradley et al., 2023).

Both the empirical and model-based approaches have enabled progress in the field. However, each has its merits and limitations. The empirical approach seeks to create a reconstruction of ice extent and dynamics through time that satisfies the available evidence. This requires potentially subjective expert interpretation, reconstructions may change as paradigms shift or more data are gathered, and this approach often lacks a direct consideration of ice physics. Conversely, the model-based approach utilises physics-based numerical models to create simulations of palaeo-ice sheet extent and dynamics. However, our knowledge of glacial processes is incomplete, meaning models are imperfect representations of reality, and approximations of ice-flow physics are often required to simulate the long timescales involved in palaeo-ice sheet modelling (Kirchner et al., 2016). Furthermore, parameter values and inputs such as past climate are often poorly constrained, necessitating models to be run multiple times to capture the likely range of uncertainty (e.g. Tarasov and Peltier, 2004; Briggs et al., 2014; Gregoire et al., 2016; Albrecht et al., 2020), or parameters to be tuned in order to create a feasible ice-sheet simulation (e.g. Patton et al., 2017). The limitations of numerical models mean that a simulation is highly unlikely to explain all the available evidence. Therefore, a long-term goal of the palaeo-ice sheet community has been to integrate these empirical and model-based approaches (Andrews, 1982; Stokes et al., 2015). Notably, some approaches have been advances in combining data on ice margins and relative sea-level data (e.g.

*Correspondence: Jeremy C. Ely, as above.
Email: j.ely@sheffield.ac.uk

Tarasov and Peltier, 2004; Gowan et al., 2021). The utility of model–data comparisons was demonstrated by Briner et al. (2020), who compared simulations of the Holocene retreat of Greenland with data on ice-margin position and timing. This led to the insight that current losses far exceed those in the palaeo-record (Briner et al., 2020). However, such quantitative comparisons are currently far from routine in palaeo-ice sheet modelling experiments.

The last British–Irish Ice Sheet (BIIS) existed from ~32 to 12 ka BP, and covered much of Scotland, northern England, Wales, Ireland and the surrounding continental shelf (Figure 1). The BIIS has been studied for over 100 years (Geike, 1894), with both empirical (e.g. Clark et al., 2012) and model-based (e.g. Boulton and Hagdorn, 2006; Hubbard et al., 2009) studies shedding light on the dynamic behaviour of the BIIS. Recently, the BRITICE-CHRONO project (Clark et al., 2021) has transformed our understanding of the BIIS. This large consortium project collected new dates for ice-sheet retreat along eight transects (Figure 1; Clark et al., 2021) culminating in a new reconstruction of the BIIS (Clark et al., 2022), supported by an extensive database of geochronological data (Clark et al., 2021) and landform mapping (Clark et al., 2018). The reconstructions by Clark et al. (2022) include empirically derived maps of the maximum, optimum and minimum ice extent through time, and ice-sheet modelling experiments tuned to fit these reconstructed ice margins at 1000-year intervals. These simulations are presented as the BRITICE-CHRONO reconstruction of growth and decay of the ice sheet (Figure 1; Clark et al., 2022). This reconstruction is currently our best simulation of the ice sheet, combining model physics and empirical data, and is useful in this regard as a benchmark simulation. However, an important point is that the model reconstruction in Clark et al. (2022) was tuned to match the empirically derived optimal ice-margin reconstructions. This required expert choices to be made in the tuning parameters and procedures; so, what other behaviours and scenarios might exist that also reasonably satisfy the empirical evidence? Here we explore, present and investigate a diversity of behavioural tendencies that occur in an ensemble of 600 ice-sheet model simulations that were permitted greater freedom to diverge from the more heavily tuned BRITICE-CHRONO model reconstruction of Clark et al. (2022). We do this because they might yield more physically realistic reconstructions for some sectors or time periods of the ice sheet (e.g. places that might have been over-tuned in the BRITICE-CHRONO reconstruction), and because it allows us to pay closer attention to more freely evolving dynamic behaviours, that could help to explain weaknesses in ice-sheet modelling approaches.

Questions and uncertainties that we address using the ensemble approach are:

1. For regions with a lower density of constraining empirical data, such as in the North Sea, what other behavioural dynamics are possible to satisfy the evidence base? Key considerations here are how, when and where did the British and Fennoscandian ice sheets meet and separate?
2. Since less empirical data are available for the build-up of the ice sheet than for the retreat, what is the range and diversity of build-up behaviours?

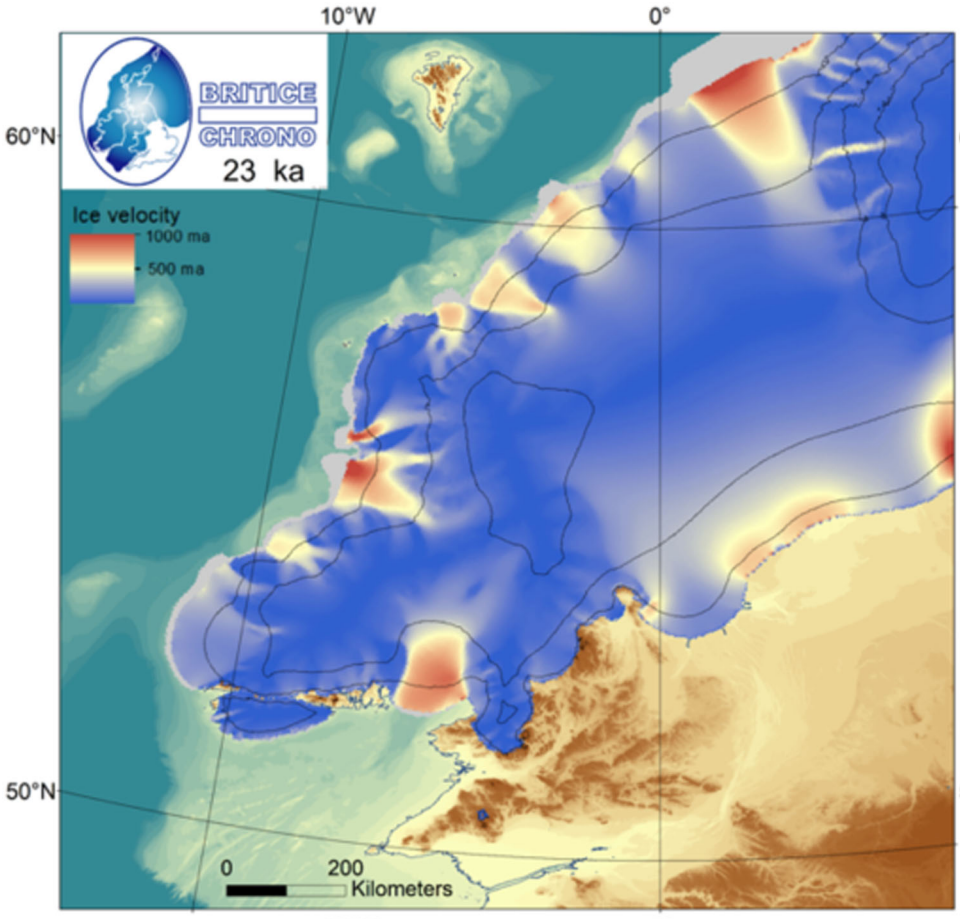

Figure 1. The BRITICE-CHRONO model reconstruction at the ice-sheet maximum volume (23 ka), from Clark et al. (2022). This reconstruction used an ice-sheet model that was tuned to approximate the empirically defined optimum ice-sheet extent (at each 1 ka time slice) and to be consistent with ice mass loading required to satisfy sea-level constraints. It therefore represents our best combined model–empirical data simulation of the ice sheet, but the tuning process to get the desired ice extents is not unique or *de facto* correct, and there may be a variety of means of achieving these extents. [Color figure can be viewed at wileyonlinelibrary.com]

3. In the BRITICE-CHRONO reconstruction (Clark et al., 2022), considerable asymmetry in the timing of growth and retreat was identified (Figure 2), with early advance and then retreat from the north-western marine sectors particularly notable. This early retreat has been attributed to ice mass loading on the continental shelf (Ó Cofaigh et al., 2021; Clark et al., 2022) and the relative sea-level rise (Simms et al., 2022) increasing water depths, and ice calving. Given the necessary simplification of these processes within a model, can this asynchronous behaviour be simulated?
4. To what extent are ice stream locations and their phases of activity fixed in time, and do any variations significantly affect retreat dynamics across sectors of the ice sheet?
5. Given that palaeo-evidence for ice shelves is difficult to derive, to what extent did ice shelves exist and influence the retreat of the BIIS?
6. What was the spatial extent and importance of ice margin readvances, and can we distinguish climate-driven readvances from internal glaciological oscillations?
7. What can our modelling say about the potential location and timing of peripheral ice caps in Britain and Ireland?

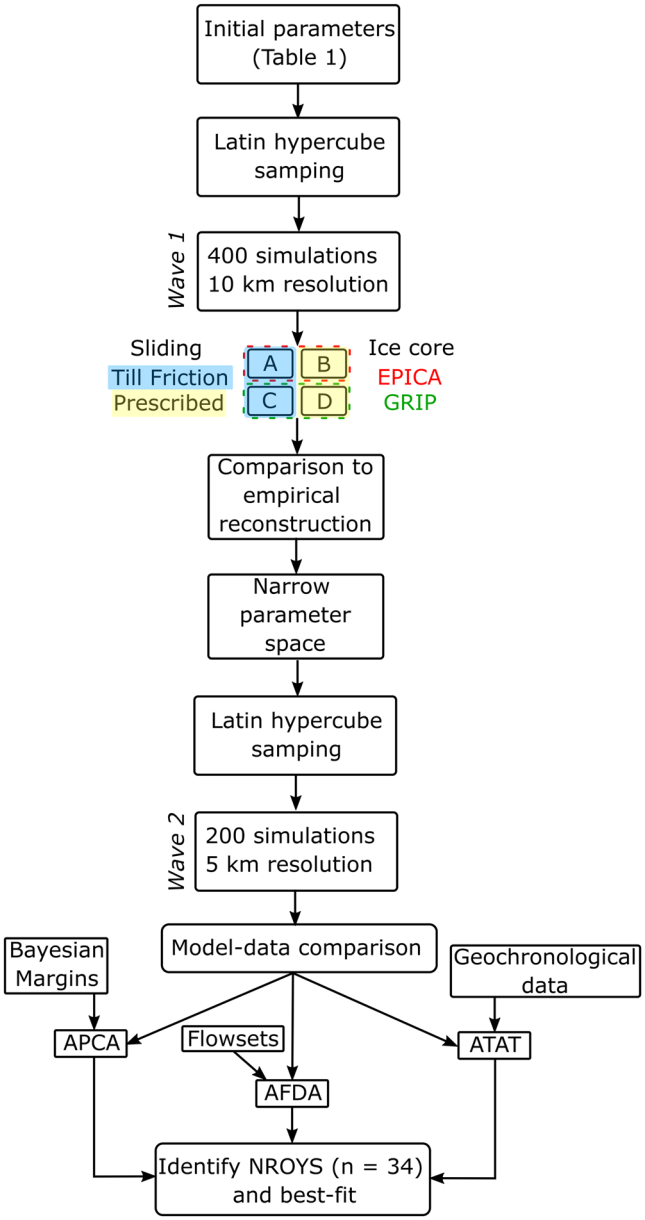

Figure 2. Flow diagram of ensemble design. [Color figure can be viewed at wileyonlinelibrary.com]

Method

Overview of ensemble design

An ensemble of 600 simulations of the last BIIS was performed using the Parallel Ice Sheet Model (PISM; see below). Figure 2 shows an overview of the ensemble design, whilst Table 1 lists the model input parameters varied in the ensemble. Further details on the role of individual parameters, model choices taken and model–data comparison techniques are described in the following sections. Here, we provide a brief overview of the ensemble procedure, which was designed to rule out simulations that do not adequately replicate observations. The application of this model-sieving procedure (i.e. progressively ruling out models), an approach often adopted in palaeo-ice sheet modelling (e.g. Briggs and Tarasov, 2013; Gregoire et al., 2016), leads to a subsection of simulations which are classified as 'not ruled out yet' (NROY) and a ranking of simulations according to their ability to fit different datasets. Notably, our approach differs from that of Clark et al. (2022), who heavily tuned to the reconstructed ice limit every 1000 years. This difference in approach, and differences in horizontal spatial and temporal resolution of the two models prevents a direct comparison.

In total, 600 simulations of the BIIS were run, each of which had perturbed input parameters covering the model aspects of ice physics, palaeoclimate and ice–ocean interactions. Parameters were sampled between minimum and maximum estimates, assuming a uniform distribution, using a Latin hypercube sampling technique (Mckay, 1992). This commonly used sampling technique efficiently explores possible input parameter values by generating combinations of parameter values that

Table 1. Ensemble parameters

	Parameter name	Main effect	Value range (experiments A–D)	Value range (experiments E–F)
Ice physics	Ice-flow enhancement factor	Deformation rate of the ice	0.5 to 1.5	0.53 to 1.46
	Sliding law exponent	Rate of basal sliding	0.001 to 1.0	0.001 to 0.663
	Maximum water thickness in till (m)	Rate of basal sliding	0.5 to 5.0	1.1 to 4.9
Climate	Temperature offset (K)	Ice sheet size and ice temperature	−3 to +3	-1.53 to 2.92
	Precipitation offset (%)	Ice sheet size	50 to 150	74 to 146
	Positive degree-day factor for snow (m/a)	Ice sheet size	0.0025 to 0.055	0.0026 to 0.0030
	Positive degree-day factor for ice (m/a)	Ice sheet size	0.0055 to 0.0085	0.0056 to 0.0082
	Forcing factor	Constraint to empirical reconstruction	0.0005 to 0.0050	0.0005 to 0.0030
Ice–ocean interactions	Calving thickness threshold (m)	Ice shelf extent	40 to 200	68.6 to 171.6
	Sub-shelf melt factor	Ice shelf extent	0.001 to 0.05	0.002 to 0.048

Table 2. Ensemble design

Set of experiments	Horizontal resolution (km)	Basal resistance scheme	Ice core record
A	10	Till friction	EPICA
B		Prescribed	EPICA
C		Till friction	GRIP
D		Prescribed	GRIP
E	5	Till friction	GRIP
F		Prescribed	GRIP

optimally fill the parameter space. Subsets of the 600 simulations utilised different modelling decisions, accounting for differing resolutions, ice-core records, and schemes for determining ice-base conditions ('Ice physics and PISM', below; Figure 2).

The ensemble was run in two waves. Due to computational time constraints, the first wave of 400 simulations was conducted at 10 km resolution. These 400 simulations were subdivided into four different experiments (A–D; Table 1) to account for the use of two different schemes for basal ice-sheet conditions (('Ice physics and PISM', below; Figure 2) and two ice-core records (Table 2; 'Climate forcing', below). Results from experiments A–D ('Simulations A–D (10 km resolution)', below) were compared with the minimum and maximum ice extents reconstructed by Clark et al. (2022) to narrow the parameter space and choose a best-performing ice-core record for the subsequent 200 model experiments ('Model–data comparison', below). These 200, which were run at a 5 km resolution and were split into two further sets of experiments (E–F), differed in their approach to determining basal yield stress (Table 2). To ensure transferability between these resolutions, two simulations with the same input parameters but varying resolutions were compared. Notably, both showed similar ice extents through time.

Simulations from the 5 km wave were compared with observational data on the ice-margin position, flow geometry and the timing of ice-free conditions, using model–data comparison tools (Ely et al., 2021; 'Model–data comparison', below). This enabled the identification of model runs that performed well against each dataset. To identify simulations that adequately replicated all the considered observational data, simulations were ruled out if they did not perform better than the mean score of an individual model–data comparison technique (Figure 2). This left a subset of 34 simulations that were deemed NROY. Though some individual simulations performed better in comparison with individual datasets, one model run was identified as 'best fit' as it was the only simulation to score in the top 85th percentile for all three model–data comparison metrics.

Ice physics and PISM

PISM is an open-source three-dimensional ice-sheet model (Winkelmann et al., 2011; The PISM authors, 2021). Experiments in this paper were performed using PISM version 1.0 with an added module for climate forcing by a glacial index method (https://github.com/sebhinck/pism-pub/tree/1.0_index_forcing; Niu et al., 2019). To model ice flow, PISM combines the shallow ice and shallow shelf approximations (SIA and SSA). The SIA dominates in the slow-flowing interior of the ice sheet, the SSA on floating ice shelves, and a combination of the two in ice streams, where speeds from the SSA exceed those of the SIA (Bueler and Brown, 2009; Winkmann et al., 2011).

Bed topography was derived from a combination of the Shuttle Radar Topography Mission digital elevation dataset onshore (https://doi.org/10.5066/F7PR7TFT), and the European Marine Observation and Data Network gridded bathymetry data offshore (https://doi.org/10.12770/18ff0d48-b203-4a65-94a9-5fd8b0ec35f6). Simulations were conducted at horizontal resolutions of 10 km and 5 km (Table 2), with 101 vertical layers within the ice quadratically spaced such that they were concentrated at the ice base. The domain covers a portion of the neighbouring Fennoscandian Ice Sheet (FIS) (to 12° E), to capture interactions between the two (Boulton and Hagdorn, 2006; Sejrup et al., 2016). The model is initialised from presumed ice-free conditions at 32 ka BP. Limited ice cover at this time is supported by ice-free dates in Scotland (Lawson, 1984; Hedges et al., 1994; Gemmell et al., 2007; Brown et al., 2007; Jacobi et al., 2009; Jardine et al., 1988; von Weymarn and Edwards, 1973; Whittington and Hall, 2002; Sutherland and Walker, 1984; Clark et al., 2022). Changes in basal topography and sea level are updated every 1000 years using the output of a glacio-isostatic adjustment (GIA) model, which accounts for the far-field effect of global ice sheets and local isostatic loading from the BIIS (Bradley et al., 2023), but is uncoupled from the simulated ice sheet. This means there may be slight inconsistencies between the ice load modelled by PISM and those used by Bradley et al. (2023) to calculate the GIA. However, this approach accounted for the effects of GIA on ice-sheet evolution, including changes in relative sea level from far-field ice sheets (e.g. Gomez et al., 2013). The rationale behind this pragmatic decision was that across the BIIS the signals from the local and far-field ice sheets are roughly equal (Bradley et al., 2023), and alternative approaches often account only for the loading of the local ice sheet. This meant that the palaeo-topography, which has been extensively calibrated against relative sea-level observations (Bradley et al., 2023), remained the same across all ensemble members.

In PISM, ice motion occurs through a combination of internal deformation and basal sliding. The rate of ice deformation ($\dot{\epsilon}$) is modelled through the Glen-Paterson-Budd-Lliboutry-Duval flow law:

$$\dot{\epsilon_{ij}} = EA(T, \omega)\tau^{n-1}\tau_{i,j}, \tag{1}$$

where E is an ice-flow enhancement factor, τ is the stress imposed on the ice, n is a flow-law exponent, and A is the ice softness. Since ice softness (A) is dependent upon the ice temperature (T) and liquid water fraction (ω), PISM models the melting and refreezing processes of temperate ice using a conservation of enthalpy-based scheme (Aschwanden and Blatter, 2009; Aschwanden et al., 2012). To account for uncertainties in the ice-flow law parameters, the ice-flow enhancement factor E is varied between ensemble members (Table 1), with the same value applied to both the SIA and SSA flows. Altering E has the effect of making the ice more or less deformable. An initial range of 50–150% was chosen for model testing.

Basal sliding is modelled using a pseudo-plastic sliding law that relates basal shear stress (τ_b) to the SSA sliding velocity (u_b) using the equation:

$$\tau_b = -\tau_c \frac{u_b}{u_0^q |u_b|^{1-q}}, \tag{2}$$

such that sliding is non-linear due to the exponent q and u_0 is a velocity threshold. This exponent also varies between our ensemble experiments, initially varying between a value of 1 corresponding to a linear sliding law and 0.001 to capture non-linear behaviour. Sliding only occurs in the model set-up when the basal shear stress exceeds the basal yield stress (τ_c). There are different schemes within PISM for determining the basal yield stress, which have a large impact on the location and velocity of ice streams (Martin et al., 2011; Peltier, 2004; Robel and Tziperman, 2016; Gandy et al., 2019). Before the full ensemble was performed, four schemes for determining τ_c were tested

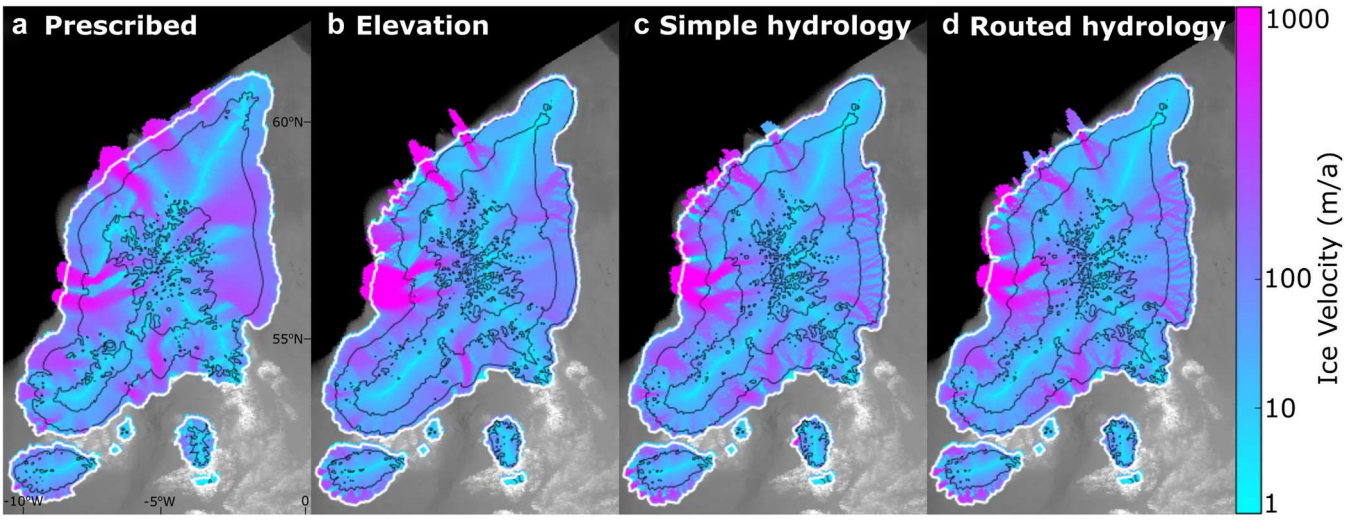

Figure 3. Modelled ice velocity at 29 ka BP using four different schemes for determining basal bed strength. The white line indicates the ice margin and/or grounding line, whilst the black contours represent surface elevation at 500 m intervals. (a) A basal shear stress map was input into the model. (b) Till-friction angle is determined by bed elevation. (c) Till-friction angle is input as a map, a local (non-mass conserving) hydrology model determines the effective pressure. (d) as in (c), but water can be routed along flow and mass can be conserved. The main difference is in ice stream width. Schemes (a) and (c) were used within the ensemble (see text for further details). [Color figure can be viewed at wileyonlinelibrary.com]

(Figure 3). The first experiment (prescribed bed) values of τ_c were prescribed depending upon the characteristics of the bed. Using the available literature, geomorphological maps and high-resolution elevation data, the bed was partitioned into five categories: (i) palaeo-ice streams, as have been reported in the literature (compiled by Gandy et al., 2019); (ii) marine sediments; (iii) thick sediments, as indicated by the occurrence of drumlins and on sediment thickness maps; (iv) discontinuous sediment, as indicated by subglacial ribs and on sediment thickness maps; and (v) bedrock, as indicated by sediment thickness maps and the characteristic rough surface evident on elevation models. The values used for each category are shown in Table 3. The remaining three schemes use a Mohr–Coulomb criterion for determining the basal yield stress:

$$\tau_c = c_0 + (\tan\phi)N_{till}, \quad (3)$$

where c_0 is the till cohesion value, which by default is zero (Schoof, 2006). This criterion required determination of two further quantities, the till friction (ϕ) and the basal effective pressure N_{till}. In the second scheme for determining τ_c (elevation dependence), ϕ was assumed to be a function of topography, with higher elevation areas having a higher till-friction angle and thus being less susceptible to sliding. For the purposes of this experiment, a tuned relationship between ϕ and elevation from the contemporary Antarctic Ice Sheet was used (Martin et al., 2011). For this elevation dependence scheme, and subsequent basal sliding experiments, a basal hydrology model is required to determine values of N_{till}. The basal hydrology model in the elevation dependence scheme considers the evolution of water thickness (W) in a layer of till beneath the ice (Tulaczyk et al., 2000; Gandy et al., 2019):

$$\frac{dW}{dt} = \frac{m}{\rho_w} - C, \quad (4)$$

where m is the rate of basal melting, ρ_w is the density of water and C is a rate at which water drains from the till layer. Basal water is not conserved in this model, and it cannot move horizontally. Instead, there is a maximum water thickness set by the user, beyond which all water is lost. In experiments that use this non-mass conserving hydrology model, this maximum thickness within the till is an ensemble parameter (Table 2), the initial range of which varied from values representing little subglacial storage (0.5 m) to large subglacial storage (5 m). The third scheme (prescribed till friction, simple hydrology), uses the same non-mass conserving hydrology model but till friction (ϕ) is prescribed according to the geomorphological map used in the first scheme. Values of ϕ applied to each category are listed in Table 3. The fourth and final scheme for determining basal yield stress (prescribed till friction, routed hydrology), used the same values of till friction according to the geomorphological map (Table 3). However, instead of the non-mass conserving simple hydrology model, a more sophisticated hydrology model was used. Here, when water thickness exceeds the maximum threshold value, excess water is routed along the modelled hydraulic potential (Bueler and van Pelt, 2015; Table 4).

Table 3. Geomorphological classification of the bed and resulting values of basal yield stress or till friction

Surface type	Prescribed τ_c, experiment 1 (kPa)	ϕ for experiments 3 and 4 (°)
Palaeo-ice stream	20	12
Marine sediment	25	15
Drumlins	60	20
Subglacial ribs	90	25
Bedrock	130	30

To ascertain which regimes for determining basal shear stress were both suitable for these experiments and produced ice stream patterns qualitatively similar to the reconstructed locations of ice streams (Gandy et al., 2019), preliminary experiments were conducted using each basal yield stress scheme. All other factors were held the same between each experiment. Results from these four simulations are shown in Figure 3. All four simulations produced similar ice extents, likely due to having the same climate and ocean forcings. Furthermore, the pattern, extent and velocity of ice streams was similar between the four simulations (Figure 3). The main region where there were large differences was in the North Sea. Here, the prescribed yield stress experiment produces broad ice streams (Figure 3a), whereas the remaining three simulations (which all use a basal hydrology model) produce a dendritic system of much narrower ice streams (Figure 3b–d). The experiments where till friction is prescribed by a geomorphological map produced near identical patterns of ice

Table 4. Overview of sliding experiments

Name	Description
Prescribed	Basal yield stress directly prescribed from geomorphological map
Elevation dependence	Till friction varies with elevation, non-mass conserving hydrology model determines effective pressure at the base
Prescribed till friction, simple hydrology	Till friction varies according to geomorphological map, non-mass conserving hydrology model determines effective pressure at the base
Prescribed till friction, routed hydrology	Till friction varies according to geomorphological map, hydrology model that routes water horizontally determines effective pressure at the base

streaming (Figure 3c–d). However, the simulation which used a routed subglacial hydrology model took approximately 30 times longer to run. Furthermore, it was decided that the simulation which depends upon basal topography to prescribe was unsuitable (Figure 3b); the basal topography evolved every 1000 years in response to the GIA, which in turn altered the basal yield stress in an unrealistic manner. Therefore, to account for the variability in determining the patterning of ice streaming between different model setups (Figure 3), and the practical considerations outlined above, the prescribed yield stress (Figure 3a) and the prescribed till friction with the simple hydrology model were used (Figure 3c). Using these two basal yield stress regimes had the added advantage of potentially determining which approach was more consistent in producing observed flow directions during our model–data comparison.

Climate forcing

Palaeoclimate is the largest uncertainty when modelling a palaeo-ice sheet (Stokes et al., 2015). Thus, a range of approaches for forcing palaeo-ice sheet models with a palaeoclimate of varying complexity have been developed (Patton et al., 2016; Tarasov and Peltier, 2004; Ziemen et al., 2019; Pollard and DeConto, 2020). The climate forcing used is often tailored to the scientific question being addressed. Computationally cheap parameterised climates allow for greater control in replicating the observed characteristics of a palaeo-ice sheet (e.g. Patton et al., 2016). However, the lack of physical processes in the climate model means that the inferences that can be made regarding the controls on ice-sheet growth and retreat are limited. In contrast, computationally expensive coupled climate–ice-sheet models directly consider climatic processes and feedback with the ice sheet (e.g. Ziemen et al., 2019). However, given the uncertainty of these processes, it would be extremely challenging for coupled models to result in a modelled ice sheet that recreates the details recorded in an empirical reconstruction. This is especially the case for the BIIS, which, due to its small size, is prone to resolution problems when using global-scale climate models (1-degree resolution). Alternative approaches include the use of climate models with low or intermediate complexity (Tarasov and Peltier, 2004), using input from an offline climate model (Gregoire et al., 2012; 2015; 2016), or a glacial index approach (e.g. Greve et al., 1999; Forsström et al., 2003). The glacial index approach scales between modern-day climate data and glacial maximum climates from a general circulation model (GCM) following a proxy record (most commonly $\delta^{18}O$ from an ice core). One disadvantage of the glacial index approach is that there is a circularity between the prescribed ice-sheet extent and elevation in the GCM and the output from the ice-sheet model (Niu et al., 2019); a similar ice sheet to the one used by the GCM is likely to be recreated by the ice-sheet model. Furthermore, the glacial index approach is likely to produce ice sheets which reach their maximum extent synchronously, at the point in time recorded to be coldest by the proxy record used. Furthermore, the indices used by glacial index methods tend to represent fluctuations in global ice volume, of which the BIIS is only a minor contributor. Since we are interested in simulating an ice sheet which resembles that of the recent reconstruction by Clark et al. (2022), and has asynchronous maximum extents in different sectors, we here adapt the glacial index approach utilising the circularity mentioned above to our advantage in the manner described below.

The modified glacial index approach adopted here adjusts between climate states at 1000-year intervals, rather than between Last Glacial Maximum (LGM) and modern-day conditions. An overview of the climate-forcing procedure is shown in Figure 4. First, a series of palaeogeographical maps were created at 1000-year intervals by combining the GIA-corrected topography from Bradley et al. (2023) with ice-sheet thicknesses from a plastic ice-sheet model (Gowan et al., 2016). This plastic ice-sheet model used the optimum reconstruction of ice from Clark et al. (2022), creating ice-sheet thicknesses that matched the reconstructed ice extent and relative sea-level record (Bradley et al., 2023). Basal shear stress values were input into the plastic ice-sheet model using the geomorphological map shown in Figure 3, using values for each mapped category as listed in Table 3. These were subsequently tuned to match the relative sea-level record (Bradley et al., 2023). Second, glacial maximum temperature and precipitation conditions were derived from multiple regression analysis of the monthly modelled LGM climates from the palaeoclimate modelling intercomparison project version 3 (PMIP3; Braconnot et al., 2012). Note that a fourth version of output from this group is now available but was released after the start of our experiments. This regression-based approach is similar to that of Hubbard et al. (2009) and Patton et al., (2016; 2017), who used modern climate datasets from which to derive regression parameters that produced spatially varying climate fields.

Our regression analysis revealed the relationships between monthly temperature and precipitation fields, and latitude, longitude, and, for temperature alone, elevation for each of the participating models over Britain and Ireland (Figure 4). All regression models accounted for >70% of the variability in the PMIP3 output. These PMIP3 experiments provide a snapshot of LGM climate, with a static LGM ice sheet which differs significantly from the Clark et al. (2022) reconstruction. To overcome this, the regression parameters were applied to palaeogeographical maps, constructed using the plastic ice-sheet thicknesses and palaeotopography provided by Clark et al. (2022). This gave temperature and precipitation fields, covering each month of the year, at 1000-year intervals, which were then offset in accordance with corresponding ice core records. To capture interannual variability between these 1000-year states, temperature and precipitation were altered according to 1000-year specific glacial indexes derived from either the GRIP or EPICA ice-core records (Figure 4b). Two records were used to test the model sensitivity to ice-core record because the EPICA core had been proven to give a better fit to the empirical record in a similar study (Seguinot et al., 2018).

To determine which of the PMIP3 climates were likely to produce a BIIS which recreated the reconstructed extent of the

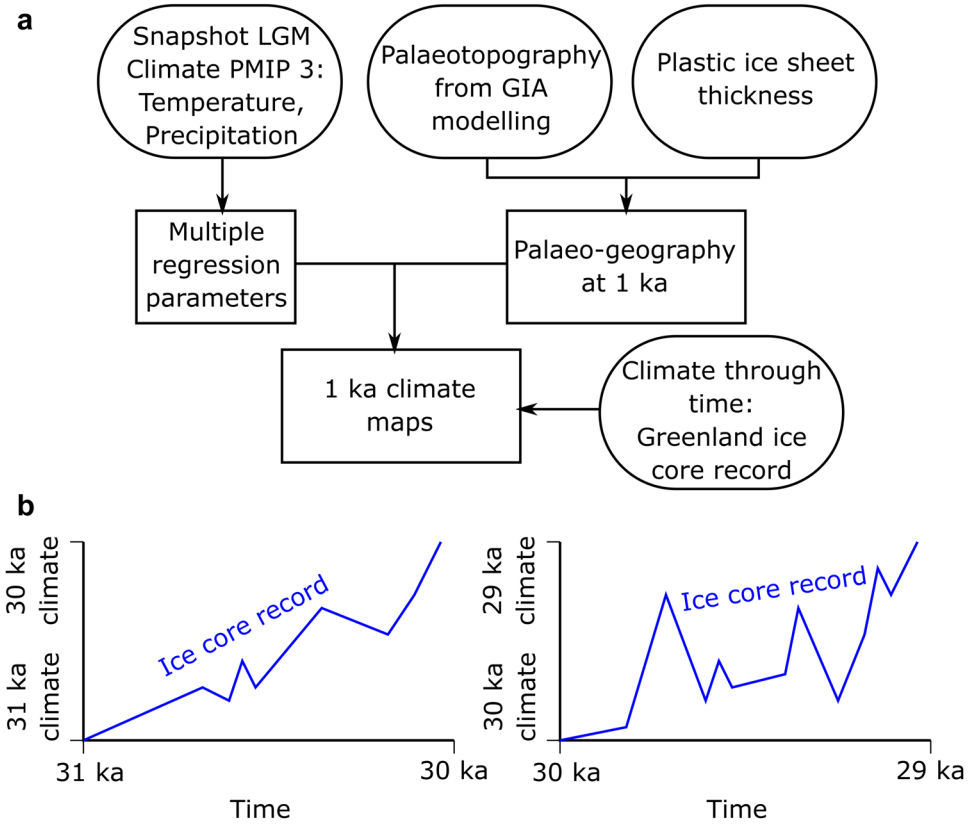

Figure 4. Climate input construction. (a) Regression parameters were derived from monthly temperature and precipitation fields at the Last Glacial Maximum, from PMIP3. These were combined with palaeogeographic maps and adjusted by an ice core record to create snapshots of climate at 1 ka resolution, which capture seasonal variability. (b) Interannual variability was captured by using a glacial index approach. Individual indexes were used to alter climate between reconstructed 1000-year states. [Color figure can be viewed at wileyonlinelibrary.com]

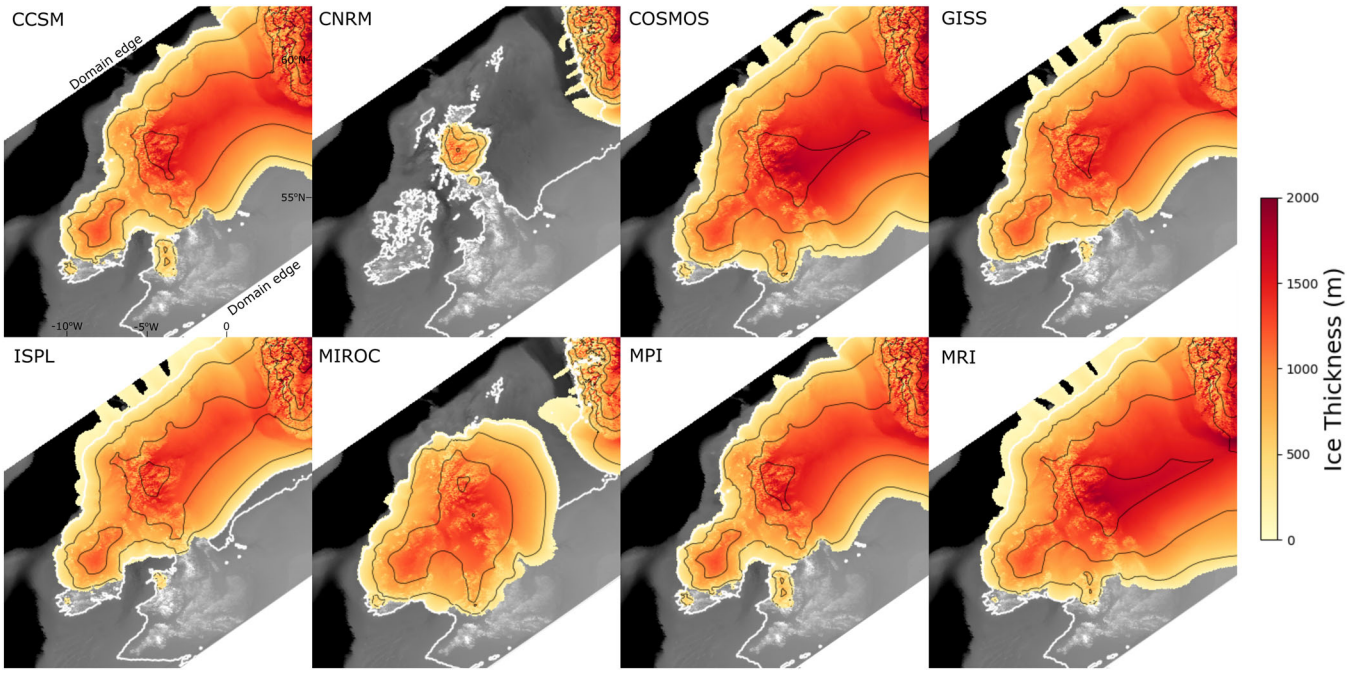

Figure 5. Simulations of the British–Irish Ice Sheet using different PMIP climates at 21 ka. Between experiments, there is a large difference in simulated ice extents and thicknesses. Note that this is unlikely to be a robust test of the climate models themselves, due to the uncertainties introduced during the processing of data for input into PISM. Dark black lines represent 500 m surface contours. Default ice-flow parameters were used in these experiments. [Color figure can be viewed at wileyonlinelibrary.com]

BIIS, we conducted a set of experiments which forced PISM with the climatic variables derived from the nine different PMIP3 experiments. Results from these experiments are shown in Figure 5. One experiment (using parameters derived from the FGOALS model) failed to complete due to creating implausibly thick ice over the domain (>6000 m). Of the remaining eight experiments, five were qualitatively deemed to reproduce an acceptable BIIS extent (CCSM, COSMOS,

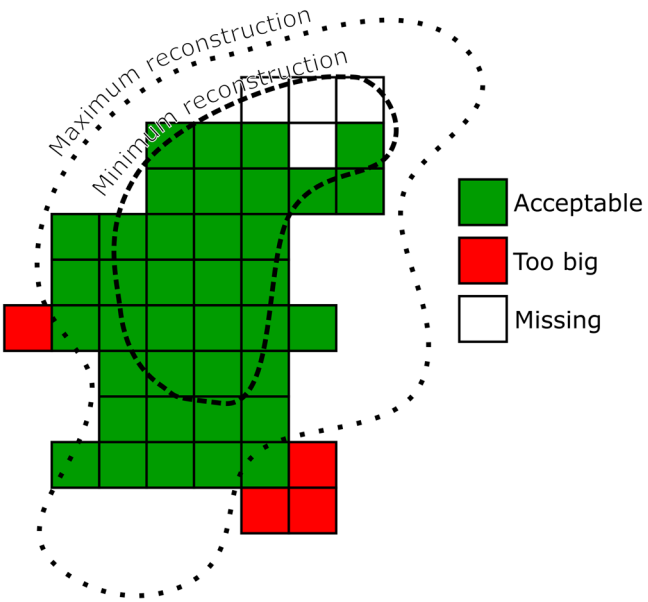

Figure 6. Overview of the 10 km model–data comparison procedure. A misfit score is calculated by summing modelled pixels that lie outside the empirically derived maximum limit ('too big') and those where ice is not modelled within the minimum empirical limit ('missing'). [Color figure can be viewed at wileyonlinelibrary.com]

GISS, ISPL and MPI), with the remaining three producing ice sheets which were too small and never coalesced in the North Sea (CNRM, MIROC, MRI). From the five experiments deemed acceptable, ensemble mean monthly temperature and precipitation fields were created. These mean values were then subjected to the procedure outlined in Figure 4, to create the input climate fields for the larger ensemble.

The resultant climatic fields were then used to drive a positive degree-day model (Calov and Greve, 2005), to convert temperature and precipitation into mass balance. This accounted for the PMIP3-modelled daily variability of surface temperature. Two ensemble parameters, one each for the rates of ice and snow melt, were varied between ensemble members (Table 2).

The bespoke climate input was further altered during the ensemble using three further ensemble parameters (Table 1). Between model experiments, temporally and spatially uniform alterations of temperature and precipitation were applied. These ranged between +/-3 K and +/-50%, respectively. Furthermore, the models were encouraged to not exceed the maximum reconstruction extent of each 1000-year time slice reconstructed by Clark et al. (2022). This was achieved by applying a surface mass flux adjustment where modelled ice that exceeded the reconstructed maximum limit for a time slice was adjusted towards zero thickness. For ease, we refer to this as a forcing factor throughout the manuscript. The forcing

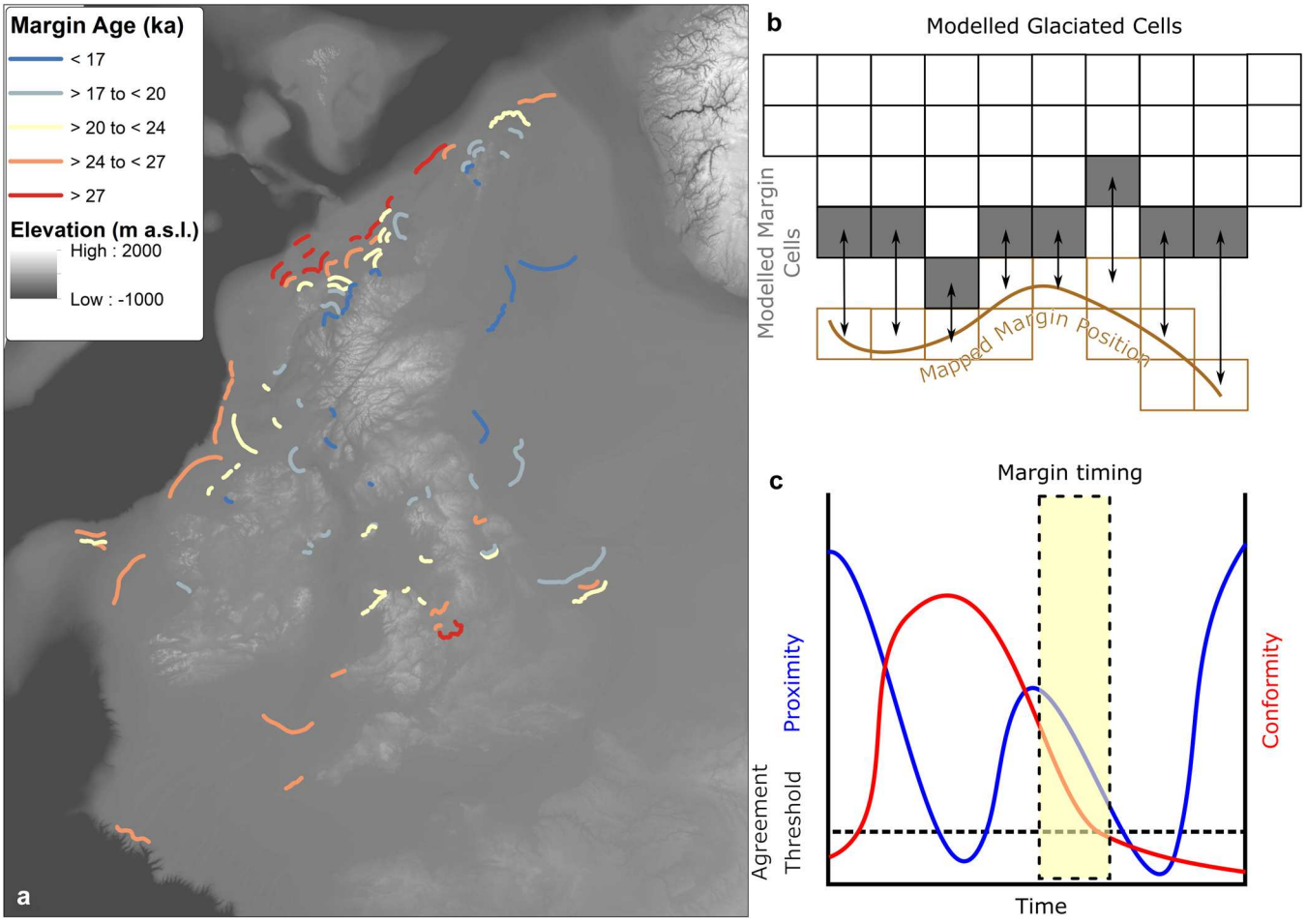

Figure 7. Overview of APCA analysis. (a) Assembled margin positions and their assigned Bayesian age. (b) The APCA procedure measures the distance between modelled margins and mapped margin positions through time, calculating the proximity (mean distance between modelled and mapped margins) and conformity (the standard deviation of distances) between the two. (c) Model–data agreement occurs when the margin proximity and conformity is below an agreement threshold during the timing of moraine occupation determined by Bayesian age analysis. [Color figure can be viewed at wileyonlinelibrary.com]

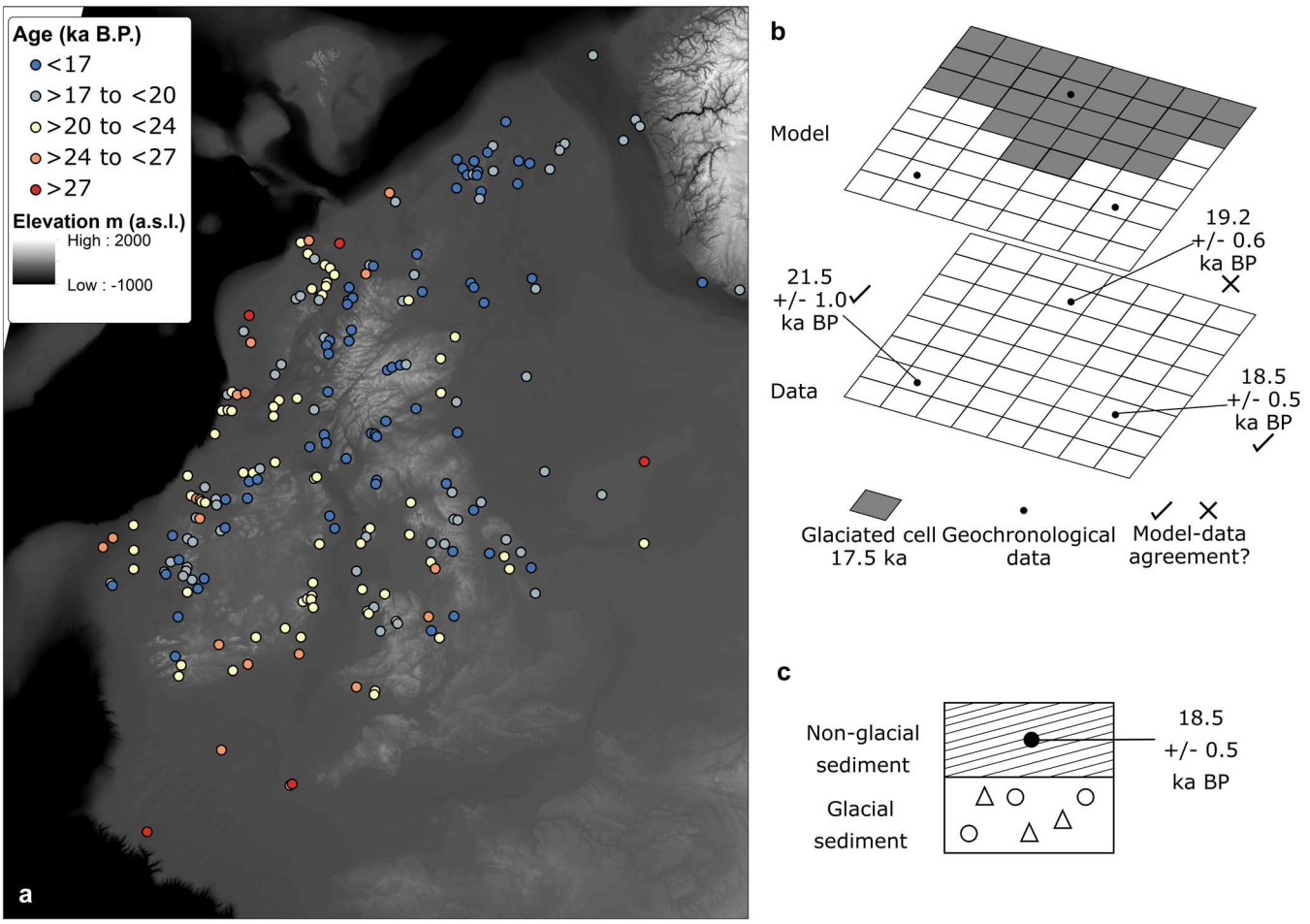

Figure 8. Overview of the ATAT model–data comparison procedure. (a) Utilised dated sites and their age range. (b) Overview of ATAT from Ely et al. (2019). In this instance, the model simulation at 17.5 ka BP correctly simulates ice-free conditions for two of the three geochronological dates. (c) All ice ages used constrain ice-free conditions (rather than advance) and were thus found in a stratigraphic setting similar to that depicted, above a glacial sediment. [Color figure can be viewed at wileyonlinelibrary.com]

factor (α) changes the amount of mass (*M*) input at the surface, causing a change in surface mass in the following manner:

$$\Delta M = \alpha(H_{tar} - H), \tag{5}$$

where H_{tar} is the target ice thickness, set to 0 outside of the maximum reconstructed ice extent which is updated every 1000 years, and H is the modelled ice thickness at a point in time. In essence, this can be thought of as increasing the amount of ablation should the model exceed the maximum reconstructed ice extent. The rate at which this adjustment occurred was determined by a further ensemble parameter that we call the 'forcing factor' (Table 1).

Ice–ocean interactions

The grounding line position is free to evolve in the model. The grounding line is determined by the flotation condition and is tracked by the model using a sub-grid interpolation scheme (Gladstone et al., 2010; Feldmann et al., 2014). Unlike previous experiments (e.g. Boulton and Hagdorn, 2006; Hubbard et al., 2009), this enabled ice shelves to occur. In a similar manner to the grounding line, a sub-grid interpolation scheme was used to track the position and stresses at the front of the ice shelves (Albrecht et al., 2011).

The model accounts for ice loss to the ocean via two mechanisms, calving and ice shelf basal melt, each of which requires a choice of model representation. Given the lack of data regarding ice shelves and ocean conditions during the period in question, we opt for simplistic representations of both processes. For calving, we adopted a thickness-based calving approach, whereby all floating ice below a certain threshold is removed. This thickness threshold is an ensemble parameter, the limits of which were initially set to a wide range to capture the uncertainty in calving rate (Table 1). For basal melt, we used the parameterisation of Martin et al. (2011), whereby sub-ice shelf temperature is set to pressure melting and basal melt rate is controlled by a rate factor – also included in the ensemble design (Table 1).

Model–data comparison

The aim of creating a model which adequately replicates data is difficult to achieve for several reasons. A hard-won datapoint collected from one location might make sense in isolation but contradict data collected subsequently or from adjacent locations (Clark et al., 2012). Furthermore, process understanding and techniques may change over time, creating contradictory data and interpretations. A more pragmatic aim, for both model-based and empirical reconstructions, is therefore to accommodate as much of the available evidence as possible. For model-based reconstructions, the fit to data can be calculated using model–data comparison tools. Such comparisons must consider the nature of evidence and taking due regard to the mismatch in spatial scales between the numerical model and the collected data (Ely et al., 2021). After such model–data comparisons, tools may be used to identify

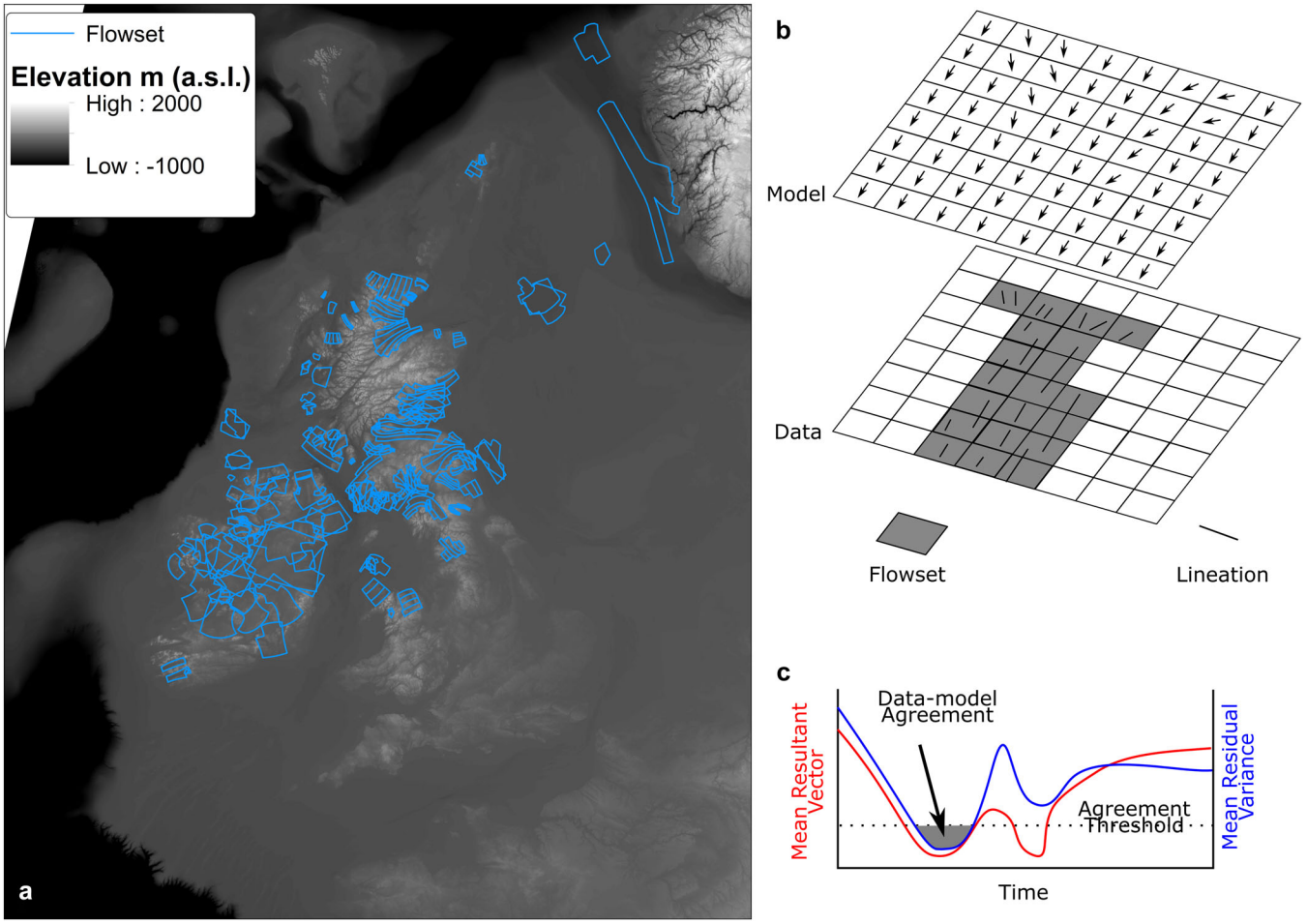

Figure 9. Overview of the AFDA model–data comparison procedure. (a) Location of flow sets of subglacial lineations tested here. (b) Overview of AFDA, which compares the shape and directional characteristics of a flow set to modelled ice-flow direction. (c) Data–model agreement for a flow set only occurs if the direction (mean resultant vector) and shape (mean residual variance) of ice flow is matched at the same time. [Color figure can be viewed at wileyonlinelibrary.com]

outlier data, the robustness of which might be questioned (e.g. Ely et al., 2019).

The aim of the first wave of 10 km simulations was to roughly rule out regions of parameter space that give ice sheets that are exceptionally too large or too small. Thus, we conducted a broad approach of comparing the simulations with the reconstructed ice limits of Clark et al. (2022). The procedure, similar to that performed by Petrini et al. (2020), is summarised in Figure 6. Here, the mismatch between the modelled and reconstructed ice extents is quantified by summing the number of modelled ice-covered pixels that are beyond the maximum limit and modelled ice-free at each reconstructed time slice. Though simplistic, we found this approach to be a quick and effective way of ruling out simulations that greatly exceeded or underestimated the reconstructed ice extents (see 'Simulations A–D (10 km resolution', below)).

The second wave of 5 km resolution simulations contained sufficient detail in the flow field and margin position to permit comparison to specific locational data. To identify NROYs from the 5 km resolution simulations, we adopted a similar approach to that outlined by Ely et al. (2021), comparing our simulations with data on margin position, flow direction and timing using three different model–data comparison tools. Modelled and reconstructed ice margin positions were compared using the Automated Proximity and Conformity Analysis tool (APCA; Napieralski et al., 2006; Li et al., 2008). Ice margin positions (97) were assembled from the sector-based reconstructions from the BRITICE-CHRONO project (Figure 7a; Bradwell et al., 2021a; 2021b; Evans et al., 2021; Chiverrell et al., 2020; Scourse et al., 2021; Ó Cofaigh et al., 2021; Benetti et al., 2021). Only margins with a clear imprint of ice-terminal landforms (identified by the BRITICE mapping in Clark et al., 2018) were used, and interpolation between features was kept to a minimum. Each margin position was assigned an age range based upon Bayesian age modelling (Chiverrell et al., 2013). APCA calculates the distance and conformity of shape between mapped and modelled moraine positions through time (Figure 7b). Agreement is said to occur if both proximity and conformity are below user-defined thresholds at a point in time (Figure 7c). In this study, thresholds of 15 km for proximity and three grid cells for conformity were used (after Ely et al., 2021). In contrast to previous work that uses APCA (e.g. Ely et al., 2021; Gandy et al., 2021), our margin analysis also considered the timing of margin positions, by only declaring a model–data match if the conformity and proximity threshold criteria were met during the time window determined from Bayesian age modelling (Figure 7c).

To compare the model runs to geochronological data pertaining to the timing of ice-free conditions, the Automated Timing Accordance Tool (ATAT; Ely et al., 2019) was used. A database of dated ice-free conditions was assembled from previous compilations (Hughes et al., 2016; Small et al., 2017) and subsequent dating from the BRITICE-CHRONO project (Clark et al., 2021). Only dates that achieved a green or amber

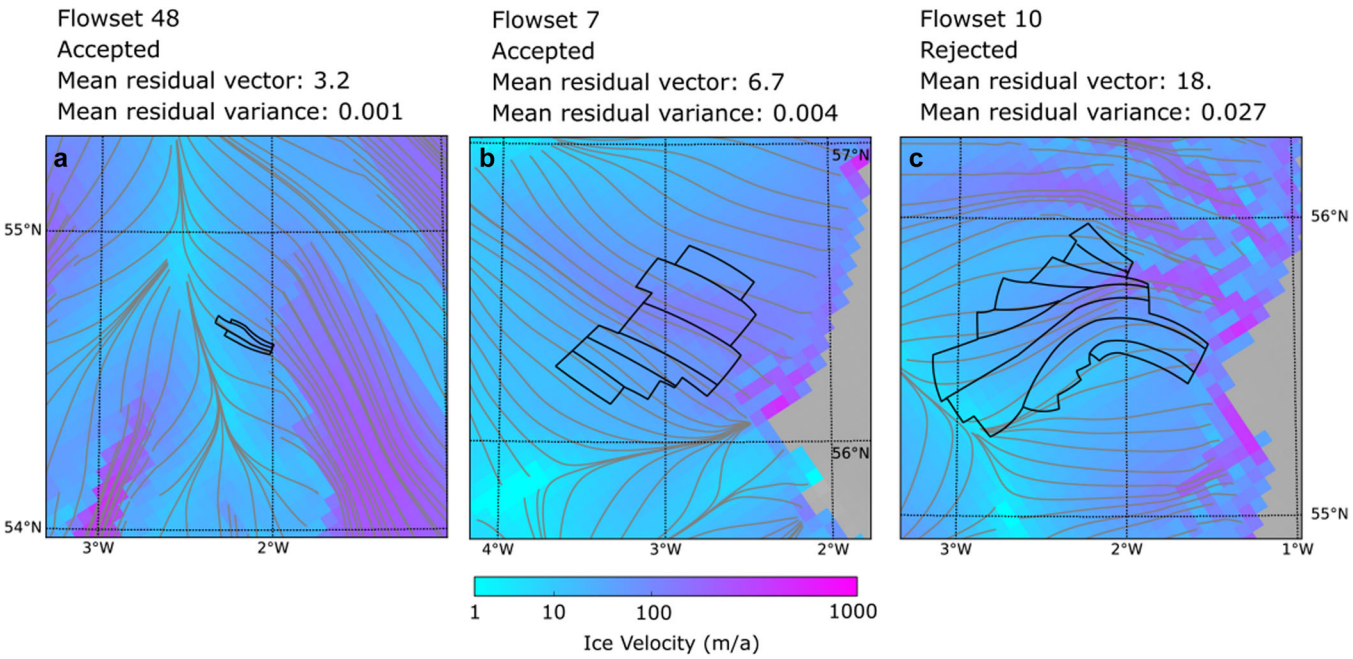

Figure 10. Examples of differing levels of agreement produced by AFDA. Black boxes show flow set locations, whilst grey lines are flowlines to aid interpretation of ice-flow directions. The flow sets depicted in (a) and (b) were accepted as matches, whilst a closely rejected comparison is shown in (c). [Color figure can be viewed at wileyonlinelibrary.com]

reliability weighting according to the criteria of Small et al. (2017) were used in our analysis, and all dates are consistently calibrated (Clark et al., 2021). Furthermore, all dates had a similar stratigraphic setting, derived either from material within sediments (for radiocarbon and luminescence dating) or boulders (for cosmogenic dating) situated on top of glaciogenic material. Given this stratigraphic setting and the quality rating given to each date, they are assumed to be the tightest available constraints on ice retreat. Some 220 dated sites were used here. ATAT calculates the number of dates that a model output agrees with, and also the time difference between the modelled and observed ice-free timings in the form of a spatially weighted root mean squared error (Figure 8b; wRMSE). The wRMSE analysis performed here accounts for uncertainty in the margin position and ice surface elevation that arises from running the model on a 5 km grid (see Ely et al., 2019 for further detail on this procedure).

Observed and modelled flow directions were compared using the Automated Flow Direction Analysis tool (AFDA; Li et al., 2007). Palaeo-ice flow directions are recorded in the landscape in the form of streamlined subglacial bedforms such as drumlins, crag and tails and mega-scale glacial lineations (Boulton and Clark, 1990; Mitchell, 1994; Ely et al., 2016). Groups of similarly orientated bedforms can be grouped into flow sets, the interpretation being that they formed during the same flow event. Some 121 flow sets were used in our analysis (Figure 9a). The flow sets were assembled from previous literature (Bradwell et al., 2007; Graham et al., 2007; Greenwood and Clark, 2009; Dunlop et al., 2010; Benetti et al., 2021; Howe et al., 2012; Hughes et al., 2014; Bradwell and Stoker, 2015; Dove et al., 2015; Ottesen et al., 2016; Van Landeghem and Chiverrell, 2020). Only flow sets that were deemed to have formed isochronously, based upon their simpler geometry and bedform imprint, were used in this analysis (Greenwood and Clark, 2009; Hughes et al., 2014). AFDA calculates the difference in flow direction between that observed and that modelled by comparing vectors on a cell-by-cell basis (Figure 9b). Where multiple lineations from the same flow set sat within a single pixel, the mean direction was used for the cell. The mean resultant vector across a flow set is used to estimate fit between modelled and observed flow directions, whilst the mean variance of vectors is used to ensure that the shape of the two flow fields is similar (Li et al., 2007). When both mean resultant vector and mean residual variance is below a user-defined threshold at a point in time, a match is deemed to occur (Figure 9c). In this study, a flow set was deemed to match when the mean resultant vector was below 10° and the mean residual vector was below 0.005 (after Ely et al., 2021). As further justification for these thresholds, Figure 10 shows examples of compared flow sets and modelled flow fields, with examples of accepted and rejected flow comparisons.

Results

Simulations A–D (10 km resolution)

The aim of our 400 simulations at 10 km resolution was to narrow the input parameter range and identify which combinations of ice core records and basal sliding regimes (in four sub-ensembles; A–D; Table 2) best fell between the minimum and maximum constraints of the BRITICE-CHRONO reconstruction of Clark et al. (2022). The 400 simulations produced a wide range of reconstructed ice extents. The left side of Figure 11 shows the full range of ice coverage from the 100 simulations of Ensemble C. To be identified as an NROY experiment, a simulation had to perform in the top 50% of misfit scores (Figure 6). From this 50%, the population of NROY simulations was halved again to those with the lowest forcing factor. The rationale of the latter being that a smaller margin forcing will have a climate input and combination of ice flow that is more in balance with the reconstructed ice extent. Table 5 summarises the results of this comparison and Figure 11 shows how the identification of NROYs improves the fit to the reconstruction.

Perhaps surprisingly, given the effectiveness of identifying model runs which match the reconstructed extent (Figure 11), this comparison procedure revealed minimal differences between the different sub-ensembles which used different ice core records and basal sliding regimes (A–D; Table 5). This is

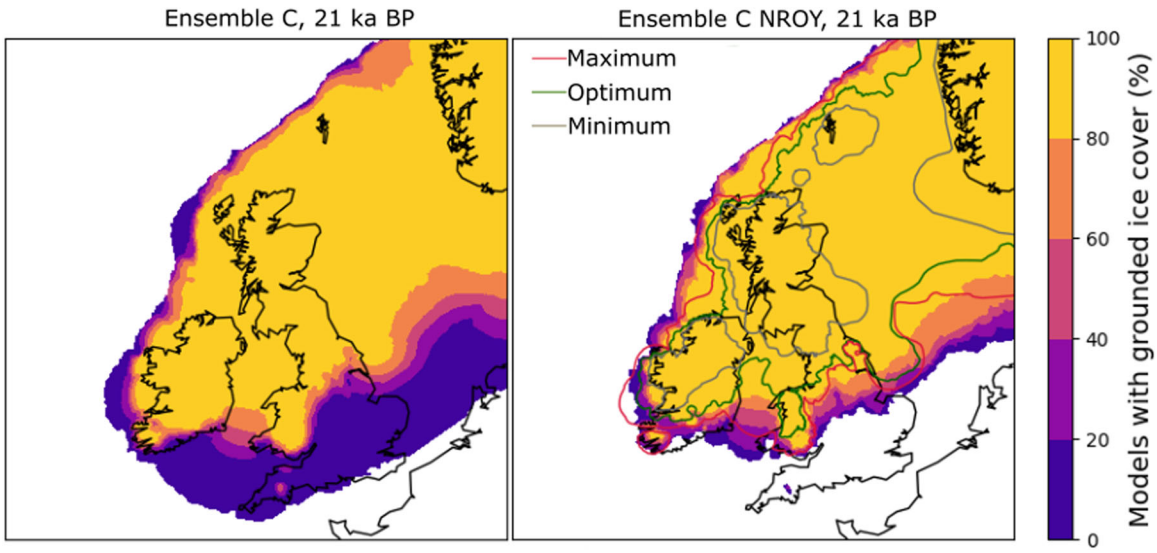

Figure 11. Results from the wave of simulations conducted at 10 km resolution. Left shows the extent of the full set of simulations from Ensemble C. Right shows only those identified as NROY simulations. The isochrones are the maximum, optimum and minimum extents from Clark et al. (2022) at 21 ka BP. [Color figure can be viewed at wileyonlinelibrary.com]

possibly due to the breadth of initial ensemble parameters, and the tendency for simulations from all four sub-ensembles to produce overly large ice sheets (reflected in large misfit scores when compared with the maximum reconstructed ice extent limit only). Both basal sliding regimes were carried forward to the 5 km ensembles, as there was no clear difference in their effect on ice extent (Table 5) and a comparison to modelled flow direction (where it is suspected different basal regimes will have the largest effect) was not undertaken at a 10 km resolution. Conversely, the minimal differences between the ice-core records revealed by this analysis (Table 5) led us to disregard the EPICA ice core, given its distal proximity to the BIIS when compared with GRIP.

The parameters used to drive the NROY 10 km simulations were used to define the range of parameters to sample for the 5 km simulations by ruling out regions of the parameter space which contained no NROY runs (Table 1). For the majority of parameters, their ranges remained similar between the 10 km and 5 km waves, with only extreme values being ruled out (Table 1). However, four ensemble parameters were significantly narrowed after this comparison. Three of the climatic parameters were narrowed. The lower bound of temperature offsets was increased from -3 K to -1.5 K (Table 1). This increase is likely caused by model runs which far exceeded the reconstructed ice extent due to too low temperatures. The lower bound of the precipitation offset was increased from 50% to 74%. Furthermore, it was found that simulations with a snow positive degree rate value of greater than 0.003 mm w.e. performed poorly, further narrowing the climatic range. Finally, one ice-flow parameter was narrowed. The upper limit of the sliding law coefficient (q) was altered from 1 to 0.66, showing that simulations closer to a linear sliding law performed poorly compared with their less linear counterparts. As the simulations with the highest forcing factors were also ruled out, the 5 km resolution simulations also have a lower forcing factor (they are less forcefully adjusted to the reconstructed ice extent). This means that the impact of this parameter is lessened in these higher resolution experiments.

Simulations E–F (5 km resolution)

Three model–data comparisons were conducted for the 5 km resolution simulations (APCA, AFDA and ATAT; see 'Model–data comparison', above). Taken in isolation, each model–data comparison technique had a different best-performing model run (Table 6): the model which best fitted one type of data didn't best-fit another type. Figure 12 shows the best-performing model run for each comparison technique at 23 ka. The time of 23 ka was chosen as the differences in North Sea glaciation (confluence or not between BIIS and FIS) are large at this time, and this is the timing of maximum ice-sheet volume found by Clark et al. (2022). Since no model performed best at all three model–data comparisons, the 'best fit' model was determined to be that which performed most consistently across the tests (described in 'NROYs and best fit', below).

Some data remained unmatched by the entire ensemble, whilst other data were matched often. Figure 13 shows the degree to which different limits were matched during the APCA comparison. On average, the simulations matched the majority of margins (Table 6), with many matched by more than 175 ensemble members (Figure 13). However, some limits were not matched by any ensemble member, notably those on the Celtic Sea shelf break, on Porcupine Bank and on the continental shelf margin west of Shetland (Figure 13). To ascertain whether these limits were not matched due to the timing constraint or the shape of the margin, a second round of APCA comparison was conducted whereby the timing comparison was removed (i.e. is the margin shape and proximity matched at any point during a model run?). This led to an improvement in fit (88.7% of margins were matched on average by the entire ensemble based on shape and proximity alone). This suggests that the addition of timing to the APCA comparison is useful for distinguishing between model runs. For

Table 5. Number of NROYs and scores for the 10 km resolution wave

Ensemble	Ice core record	Basal resistance scheme	Mean misfit score		Number of NROYS
			Full ensemble	NROY	
A	EPICA	Till friction	37976	28537	15
B	EPICA	Prescribed	36725	26337	18
C	GRIP	Till friction	34928	29098	16
D	GRIP	Prescribed	34803	28144	17

Abbreviation: NROY, not ruled out yet.

Table 6. Summary of model–data comparison results

Model–data comparison tool	Scores			
	Ensemble mean	NROY mean	Best-fit individual tool	Overall best fit
APCA number of margins ($n = 97$)	40 (41.2%)	51 (52.6%)	63 (64.9%)	53 (51.4%)
AFDA number of flow sets ($n = 121$)	41 (33.9%)	44 (36.4%)	51 (42.1%)	46 (38.0%)
ATAT number of dates ($n = 220$)	130 (59.1%)	148 (67.4%)	189 (86.0%)	160 (72.7%)
ATAT wRMSE (years)	883	565	663	495

Abbreviations: AFDA, Automated Flow Direction Analysis; APCA, Automated Proximity and Conformity Analysis; ATAT, Automated Timing Accordance Tool; NROY, not ruled out yet; wRMSE, weighted root mean squared error.

the specific examples above, when timing isn't considered, the limit west of Shetland showed an improved fit to the models (95% model runs replicated proximity and shape). However, the limits on Porcupine Bank and the Celtic Sea shelf break did not produce a model–data match based purely on limit shape and proximity. This persistent model–data mismatch was due to no model runs reaching the extent (a close enough proximity) indicated by these limits.

The number of times an ensemble member matched a date according to ATAT is also shown in Figure 13. The majority of dates were matched by more than 150 experiments (100 dates), or 100 ensemble members (an additional 32 dates). Notably, there are several regions where dates were matched less often by ensemble members. Of the 220 dates in total, only four produced no matches across the ensemble. This includes two sites from central Scotland (Phillips et al., 2006; Ballantyne et al., 2009; Everest and Kubik, 2006), Gallowflat in Scotland (McCabe et al., 2007) and an OSL date from a site in the North Sea (Roberts et al., 2018). There are also notable regions of model–data mismatch (Figure 13), including coastal sites around east Ireland, sites on the western continental shelf and western Scotland.

The degree to which different models matched data across for different flow sets also varied according to AFDA. When considering the best match across the entire ensemble, some flow sets were matched with a corresponding modelled flow direction of 2°, whilst others never achieved a model–data offset of less than 25° (Figure 13). There appears to be no spatial pattern to distinguish between the best and worst matched flow sets, nor does flow-set size correspond to the degree of matching (Figure 13). Perhaps of interest is that flow sets on flat terrain (e.g. central Ireland, the North Sea) were among some of the best matched flow sets, suggesting that the model was able to recreate flow directions even where there was a lack of topographic steering. In accordance with Ely et al. (2021), flow sets remained a difficult constraint for the model to match, with models generally only matching 33.9% of flow sets (Table 6).

NROYs and best fit

Ensemble members from the 5 km ensemble were deemed to be a NROY simulation if they surpassed all of the following thresholds for each model–data comparison tool, determined by visually assessing the fit between model simulations and data:

- A spatial and temporal match to more than 40 margins, using APCA. These simulations were visually deemed appropriate in both spatial extent, pace and timing of retreat.
- A flow direction match to 42 or greater flow sets, determined using AFDA. These simulations appear to recreate the main flow patterns of the BIIS.
- Accordance with greater than 60% of the dates, with a wRMSE of <850 years across the dataset. This percentage threshold produced simulations that accounted for the correct deglaciation of the majority of dated sites, whilst the temporal error allowance was deemed reasonable given the spread of uncertainty on available geochronological data (often in excess of 1000 years).

Though guided by our interpretation and soft knowledge of the BIIS, these thresholds are ultimately subjective, and future work should focus on more statistically robust means of identifying NROYs.

In total, 34 simulations were deemed to be NROYs, each of which scored within the top 50th percentile for all three model–data comparisons. Of these 34 simulations, 19 came from sub-ensemble experiment E (which used the till-friction approach to defining basal yield stress) and 14 came from sub-ensemble experiment F (prescribed basal yield stress). On average, these NROYS displayed a model–data match for 51 (52.6%) margins, 44 (36.4%) flow sets, and 148 (67.4%) dates with a wRMSE of 565 years (Table 6). The best-fit model was defined as the model which performed most consistently well across the three model–data comparison techniques. Only one model was in the top 85th percentile for all three tests, matching 53 (51.4%) margins, 46 (38.0%) flow sets and 160 (73%) dates with a wRMSE of 495 years (Table 6). Table 7 shows the range of parameters input into the NROY simulations, as well as those used for the best-fit simulation. For most parameters, selecting only the NROYs does not significantly narrow the input range (full range in Table 1; NROY parameters, Table 7). However, a slight narrowing of the temperature offset (minimum -1.53 K input to -0.73 K in the NROYs) and further reduction of the basal sliding law exponent (maximum 0.66 input and 0.52 in the NROYs) arose from the selection of NROYs.

Discussion

Our free-running modelling experiments capture many of the characteristics of the ice sheet in the BRITICE-CHRONO model reconstruction (Clark et al., 2022), allowing us to use the various model experiments to discuss the ice sheets' potential dynamics, especially at times and places where there is good model–data agreement. Given the difference in spatial and temporal resolution (2.5 km and 1 ka, respectively, in Clark et al., 2022) and approach, we refrain from quantitative comparison with the BRITICE-CHRONO simulation, instead discussing broad patterns of agreement/disagreement and regions of data that were considered by that reconstruction. Selected time slices of ice-sheet model evolution from the NROY experiments are show in Figure 14, including differences in model predictions. A figure which shows each 1 ka time slice is included in the supplement (Supplementary Figure 1), and these may be useful for future endeavours to reconstruct the ice sheet, especially if aspects of the BRITICE-CHRONO model reconstruction are found wanting. The volume and area of NROY simulations through time is shown in Figure 15. Furthermore, Figure 16 shows the

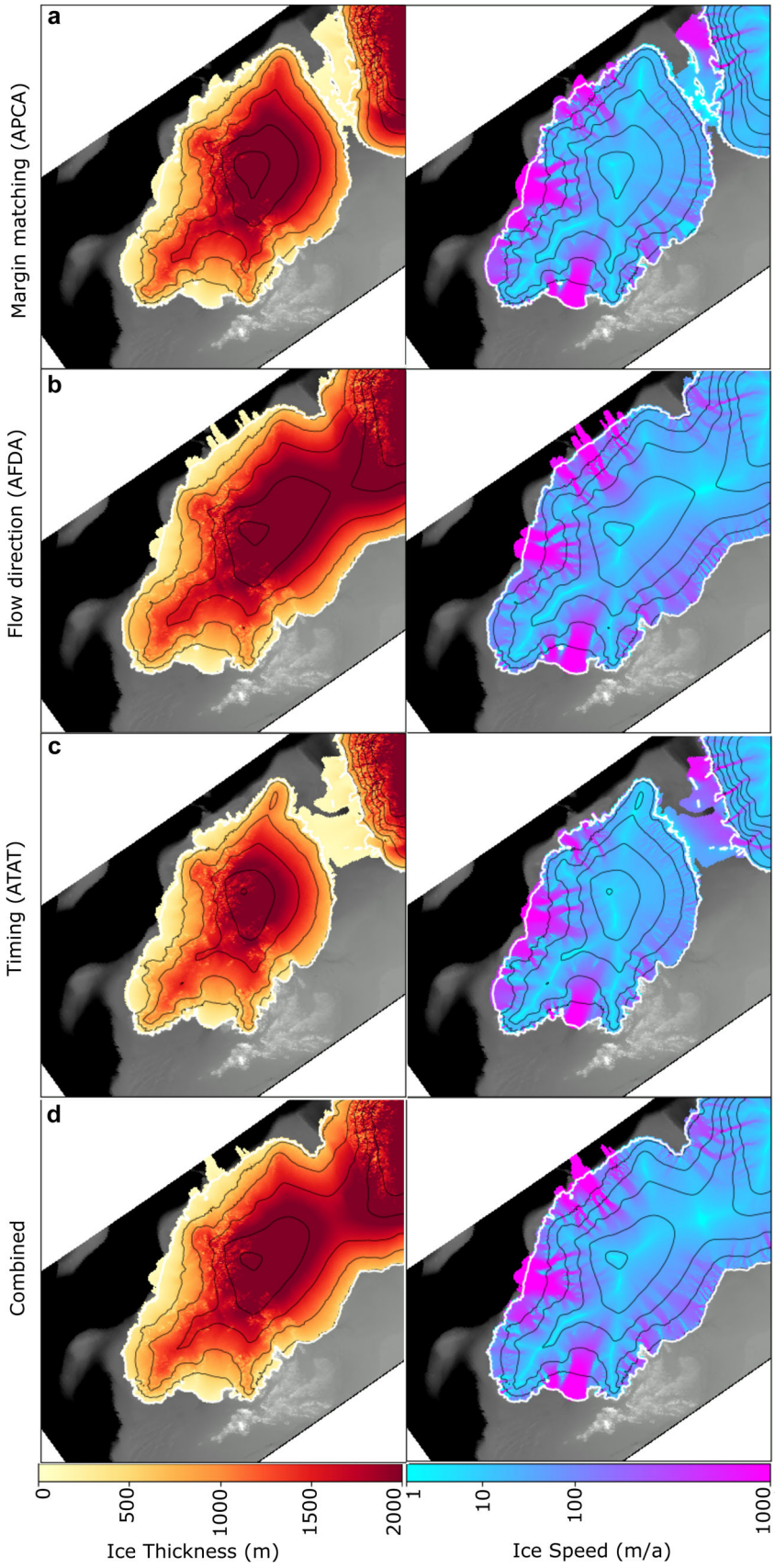

Figure 12. Best-performing models according to the model–data comparison at 23 ka BP. (a) Best-performing model according to margin matching (APCA) only. (b) Best-performing model according to flow direction (AFDA) only. (c) Best-performing model according to timing (ATAT) only. (d) Best-fit simulation overall, combining scores from all three model–data comparison tools. [Color figure can be viewed at wileyonlinelibrary.com]

best-fit simulation compared with the minimum, optimum and maximum reconstruction limits of Clark et al. (2022). Qualitatively, the models perform well at replicating the empirically reconstructed behaviour of the BIIS (Figures 14 and 16), as is also reflected in the model–data comparison scores for empirical margins and timing constraints (Table 6). Briefly, this includes the placement of the major ice stream outlets (Figure 1), shelf-break glaciation and coalescence/retreat to smaller ice caps (Clark et al., 2022). In this discussion, we use these NROY simulations to address the questions posed in the introduction, highlighting the range of potential ice dynamics produced by our model.

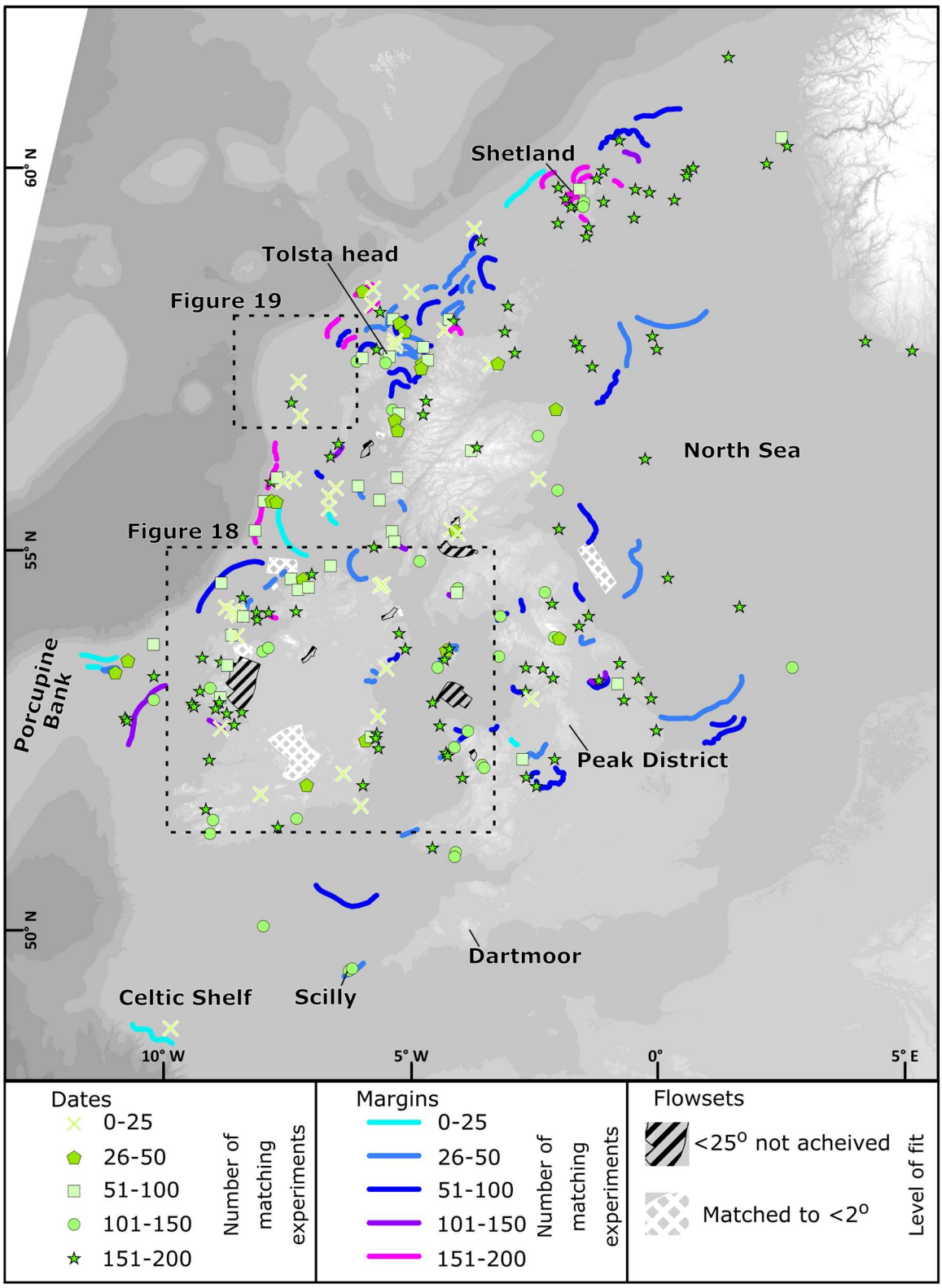

Figure 13. Results from the model–data comparison, showing the degree of fit between the ensemble of simulations for the tested dates, margin positions and flow sets. [Color figure can be viewed at wileyonlinelibrary.com]

Dynamic behaviour in data-poor regions

Despite being a densely studied palaeo-ice sheet, three regions stand out as being comparatively data poor, namely: (i) the North Sea (Figure 17), where Holocene sediment covers much of the glacial geomorphology, making recovery of datable material challenging; (ii) central Ireland (Figure 18), which has a rich geomorphological record, but comparatively few geochronological dates; and (iii) the offshore region west of the Outer Hebrides near St Kilda (Figure 19). Since these regions are the least constrained by data in our NROYs, they produce a wide range of dynamic behaviour, which we highlight here to inform future reconstructions and guide further data collection.

The North Sea is the largest of the three areas outlined above and is the site of the coalescence and splitting of the BIIS and FIS (Sejrup et al., 1994; Boulton and Hagdorn, 2006; Clark

Table 7. Parameters of NROY and best-fit simulations

	Temperature offset (K)	Precipitation offset (%)	Forcing factor	PDD snow (m w.e.)	PDD ice (m w.e.)	Calving thickness (m)	Basal sliding exponent	Ice-flow enhancement factor	Sub-shelf melt factor	Till thickness (m)
NROY min	−0.74	0.68	0.0006	0.0028	0.0061	71.8	0.0015	0.54	0.002	0.82
NROY max	2.88	1.39	0.0030	0.0054	0.0082	196.5	0.5184	1.46	0.047	4.76
Best fit	2.61	1.08	0.0030	0.0044	0.0072	140.0	0.0047	1.43	0.008	2.74

Abbreviations: NYRO, not yet ruled out; PDD, positive degree-day.

et al., 2012). Few studies have depicted the coalescence between the two ice sheets, with many reconstructions starting from the timing of maximum extent. This is probably a consequence of the limited empirical data constraining ice behaviour at this time. It is also worth noting the complexity in modelling this region, as was highlighted by Patton et al. (2016), whose optimum model was unable to achieve both a full North Sea ice cover and realistic deglaciation. In a set of bespoke experiments, Boulton and Hagdorn (2006) modelled a scenario whereby the BIIS and FIS collided in the central North Sea and built an ice divide between western Scotland and southern Scandinavia. Based on a reinterpretation that dates taken from the cores of Sejrup et al. (1994) in the central North Sea constrain ice advance, Clark et al. (2022) depicted the BIIS and FIS joining further south in the North Sea (just north of Dogger Bank), with an ice divide migrating northwards as it grew in elevation.

The NROY models produce two main scenarios for BIIS and FIS coalescence (Figure 17a and b). We note that in both scenarios, North Sea ice cover is predominately sourced from the BIIS. One possibility is that this is due to the Norwegian Channel Ice Stream diverting FIS-sourced ice, preventing its advance over the North Sea (Clark et al., 2022). Alternatively, this may reflect the limited model domain over the FIS region, though we note a similar BIIS coverage of the North Sea also occurs in the simulations of Patton et al. (2016), in which the entire FIS domain is covered. The first scenario (Figure 17a) is similar to the model of Boulton and Hagdorn (2006), whereby the two ice sheets meet in the central North Sea and grow to build an ice divide. In the second NROY scenario, the ice sheets meet via floating ice shelves, rather than by grounded ice (Figure 17b). Indeed, in some simulations, thick ice shelves flowing from Norway toward Scotland are predicted to ground on high points in the sea floor (e.g. the Tampen ridge, Figure 17b). Such simulations raise the possibility of ice shelves being important in the coalescence of the two ice sheets.

The separation of the BIIS and FIS has been reconstructed more frequently. Broadly, two scenarios of separation have been suggested: (i) the development of a large calving bay to the west of the Norwegian Channel Ice Stream, with ice on the continental shelf retreating into deeper bathymetric lows whilst the Norwegian Channel Ice Stream remained at shelf break (Carr et al., 2006; Bradwell et al., 2008); and (ii) an 'unzipping' of the two ice sheets, due to retreat of the NCIS (Sejrup et al., 2016; Merritt et al., 2017; Hjelstuen et al., 2018; Gandy et al., 2021; Clark et al., 2022), the timing of which is debated in Evans et al. (2021).

As with the modelling study of Gandy et al. (2021), none of our simulations produce the calving-bay style of deglaciation. Some of our simulations reproduce the unzipping via the retreat of the NCIS scenario (e.g. Figure 17c and d). In most of our simulations, however, retreat occurs both in the southern North Sea and along the Norwegian Channel. This is unlike the simulations of Gandy et al. (2021), where the unzipping of the ice sheets is solely driven by grounding line retreat of the NCIS. When an unzipping scenario of separation is simulated, the location of separation always occurs near to the NCIS, but the latitude varies (a more northerly separation is shown in Figure 17c and d than in Gandy et al. (2021)). An alternative scenario, which to our knowledge has yet to be proposed in the literature, is demonstrated in Figure 17e and f. Here, retreat occurs on both the north and south flanks of the North Sea divide, and in the north leaves behind an independent ice cap over Shetland (broadly consistent with that reconstructed by Bradwell et al., 2021a). Interestingly, the thinning of the main North Sea Ice Divide results in the two ice sheets being 'bridged' by an intermediate ice dome (Figure 17e) which in some simulations becomes isolated, leaving an independent ice cap in

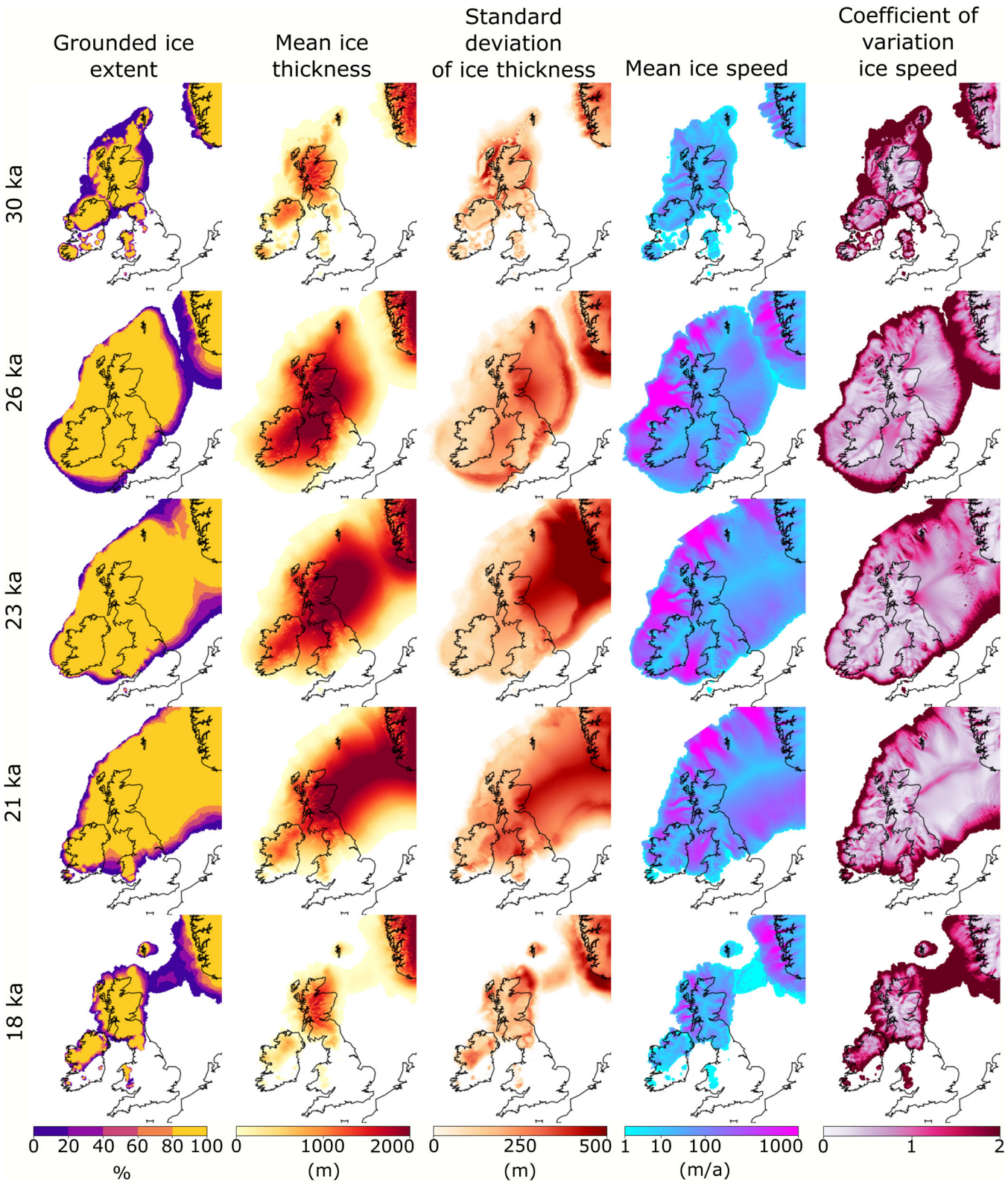

Figure 14. Summary of NROY simulations. From left to right, these show the percentage of NROY simulations that have ice cover, the mean ice thickness, the standard deviation of ice thickness, the mean ice speed and the coefficient of variation of ice speed. [Color figure can be viewed at wileyonlinelibrary.com]

the North Sea (Figure 17f). This ice cap in these simulations is short-lived, probably due to being completely marine-based and lacking high enough elevations over which to accumulate snow. The accuracy of this ice bridge scenario awaits further examination of the geomorphological and geochronological record, and we here propose it as being feasible given the data–model comparison we have conducted to leave these NROY simulations. A further consideration for future work is the role of the ice-dammed lake that occurred in the southern North Sea (Hjelstuen et al., 2018). Proglacial lakes are not included in our model, but have been shown elsewhere to increase ice-retreat rates (Hinck et al., 2022). Whether an 'unzipping' or an 'ice bridge' scenario occurs is dependent upon the type of sliding regime prescribed (see 'Ice physics and PISM', above). The unzipping scenario occurs when basal resistance is prescribed, whilst when basal resistance is dependent upon the till-friction

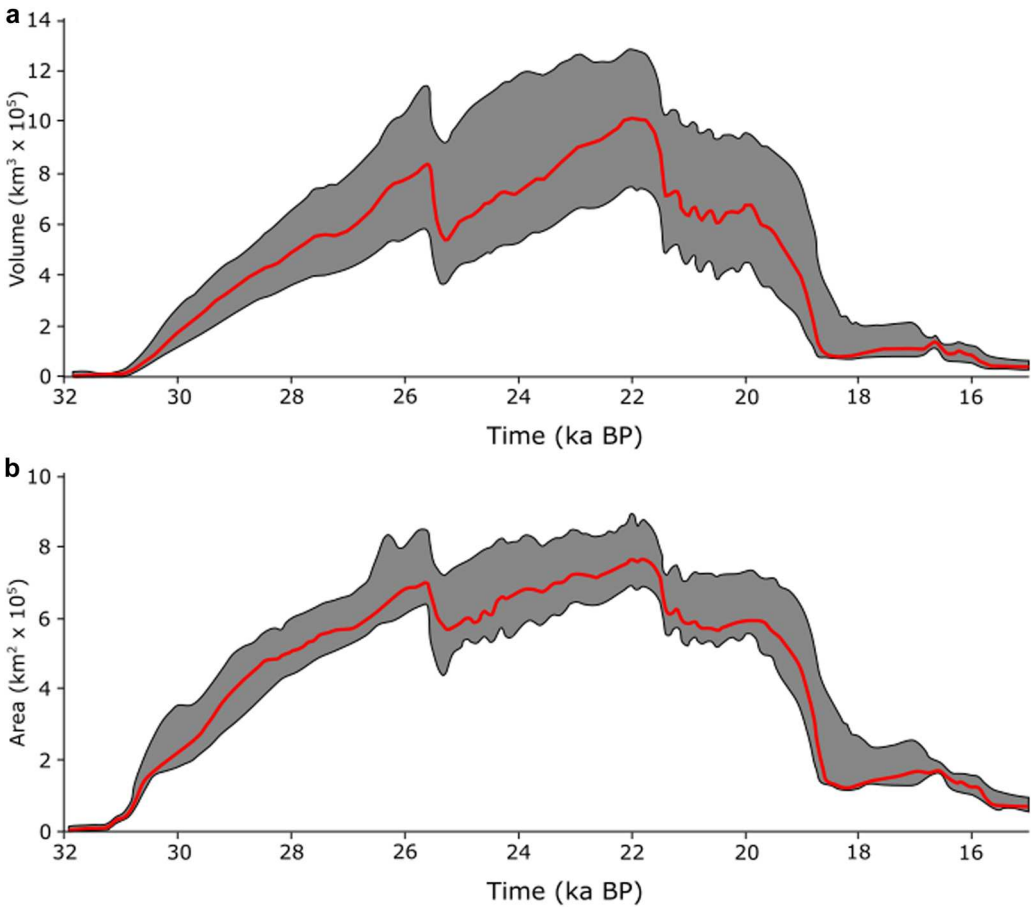

Figure 15. The volume (a) and area (b) of the NROY simulations through time. The upper and lower black lines represent the maximum and minimum values. The red line is from the best-fit NROY simulation. Note that the domain encompasses part of the Fennoscandian Ice Sheet. [Color figure can be viewed at wileyonlinelibrary.com]

angle, an ice bridge arises. This case study of the North Sea deglaciation demonstrates how the style, position and geometry of retreat are impacted by the type of sliding regime utilised in our simulations, underscoring the importance of robustly describing basal conditions for ice-sheet modelling. The exact effect of this is difficult to determine, since the pattern and degree of basal sliding impact ice elevation, which in turn has ramifications for climatological, ice dynamical and ice–ocean components of the ice sheet.

In north and central Ireland, three common qualitative modes of behaviour arise in various model simulations, with transitions between modes occurring. Retreat of the Irish Sea Ice Stream often leads to separation of British and Irish ice and the development of an independent Irish Ice Sheet with a narrow ice-free corridor adjacent to and west of the North Channel, and with a single ice divide configuration (Figure 18a). This model result differs from previous empirical reconstructions, which attributed the single divide structure to periods of time when the Irish Ice Sheet was still attached to the remainder of the BIIS (e.g. Greenwood and Clark, 2009; Clark et al., 2012). During the course of some model runs, the resultant Irish Ice Sheet exhibits two, or even three, domes from which ice radiates (e.g. Figure 18b and c). The dual-domed scenarios also resemble previous empirical reconstructions (Figure 18b; Greenwood and Clark, 2009). In a tri-dome scenario, an additional divide forms between these two (Figure 18c). In the final modelled stage of deglaciation in Ireland, the Irish Ice Sheet separates into separate ice caps (Figure 18d). The largest and most prevalent of these are situated over Connemara and centred in Northern Ireland, consistent with regional reconstructions (e.g. Wilson et al., Greenwood and Clark 2009). Note that the model simulations correctly deglaciate the Cork–Kerry Ice Cap in south-west Ireland before the ice domes further north (e.g. Figures 16 and 20 ka), consistent with the reconstruction of Clark et al. (2022) based on dating evidence (Barth et al., 2016). During a single model run, the divide structures can alter between these single- to tri-dome states over the course of only a few centuries, suggesting that the flow configuration of the Irish Ice Sheet was more complex than previously reconstructed. Overall, these model results lend physical plausibility to the empirical reconstructions of ice divide configurations during deglaciation. The lack of dates in these areas means that the primary data constraint here is flow sets (e.g. Greenwood and Clark, 2009) of subglacial lineations. In the absence of dated constraints, future experiments which focus primarily on the deglaciation of Ireland may want to weight the evidence from flow sets more highly than other forms of evidence.

Model predictions in the offshore region west of the Outer Hebrides are less variable than for the other data-poor regions. Here, NROYs produce a short-lived advance of ice to the continental shelf break, reaching a maximum extent at approximately 29 ka BP (Figure 19a) and then early retreat across the region with this portion of the continental shelf remaining ice-free for the remainder of a simulation (Figure 19b). Offshore evidence for past glaciation in this region is limited to moraines on the shelf break (e.g. Bradwell et al., 2008) and an ice-free radiocarbon age (Peacock et al., 1992; calibrated to 26.3 ka +/- 0.3 ka by Hughes et al., 2016). These two lines of evidence are reasonably consistent with our NROY predictions; two of the three sets of moraines align well with the small ice

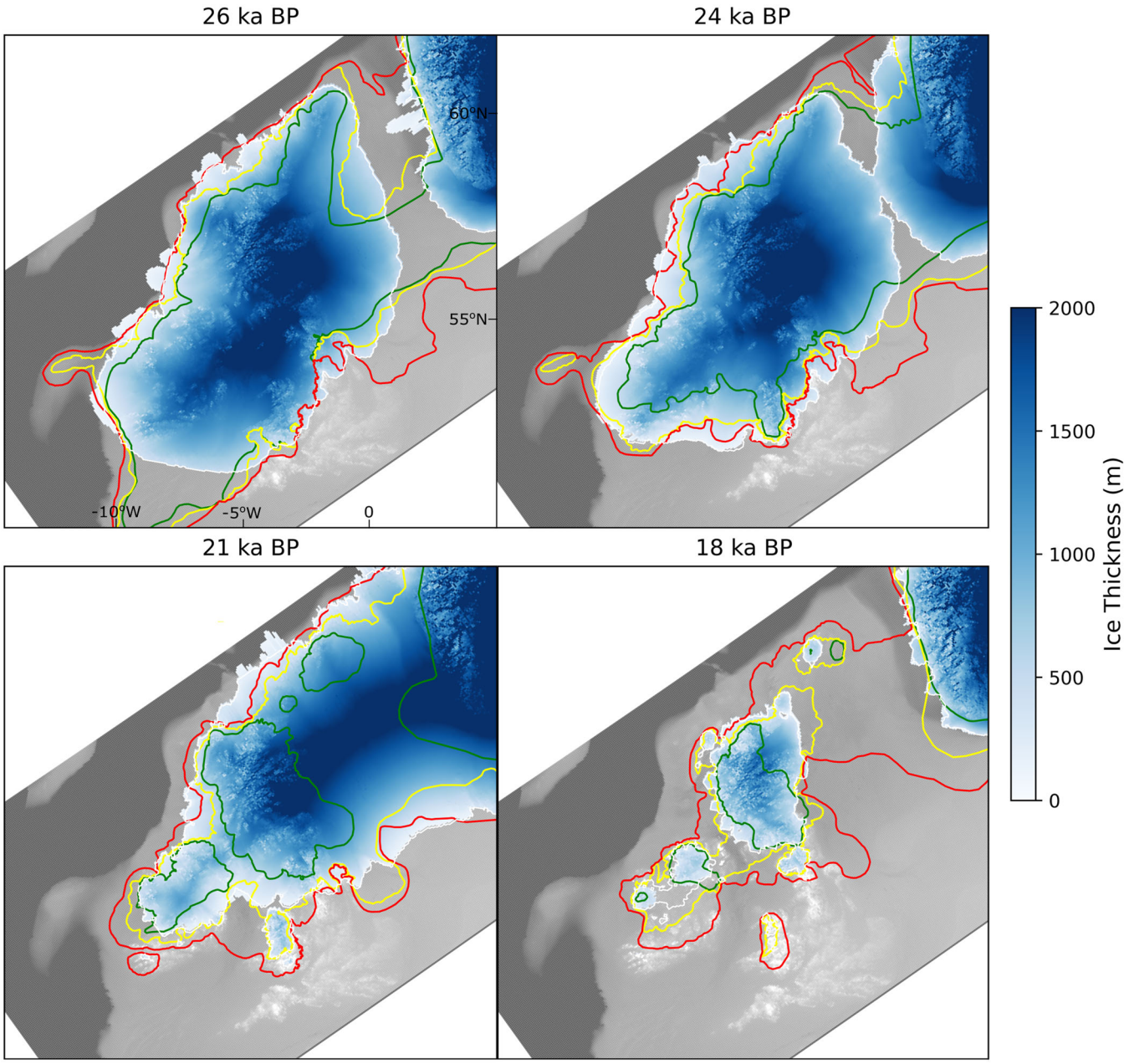

Figure 16. Ice thickness of the best-fit simulation compared with the minimum (green line), optimum (yellow line) and maximum (red line), reconstructions from Clark et al. (2022). [Color figure can be viewed at wileyonlinelibrary.com]

streams simulated by our models (Figure 19a), and NROYs predict ice-free conditions at this time (Figure 19b). However, the NROYs contradict additional data available from the St Kilda archipelago, where stratigraphy and geomorphology preserved from previous glaciations (Sutherland and Walker, 1984; Hiemstra et al., 2015), as well as cosmogenic dating at ~290 m altitude, suggest that the BIIS did not overrun the Island of Hirta, where St Kilda is located (Ballantyne et al., 2017). In contrast, our models produce ice that would have subsumed the peaks of St Kilda with approximately 200 m of ice. This apparent model–data discrepancy may be a consequence of: (i) a failure of the model to correctly predict ice thickness in the region; (ii) the geomorphological evidence of older glaciations on St Kilda being preserved under the thin, short-duration ice cover, as our model produces; and/or (iii) the inability of the model to resolve small topographic highs such as St Kilda may lead to their effect on ice flow being underestimated, and thus the model is unable to simulate them as nunataks (Mas e Braga et al., 2021).

Dynamics during ice-sheet growth and asynchronous behaviour

Evidence for the build-up of the BIIS to its maximum extent is less abundant than for its well-constrained retreat. This is due to the poorer preservation potential of this older evidence, especially given the overriding of the ice sheet itself. Therefore, the dynamics of the ice sheet during the build-up phase are less well constrained compared with the retreat. An emerging pattern though is that the maximum extent was reached asynchronously (Clark et al., 2012, 2022) around the ice sheet's perimeter. We therefore loosely define the build-up phase as the period between 32 and 23 ka BP, and which varies by sector of the ice sheet.

All NROYS demonstrate a rapid increase of ice volume (Figure 15) from the ice-free state we prescribe at 32 ka to form an ice cap over Scotland at 31 ka. The choice of an ice-free state at this period is a pragmatic one. Indeed, during this period, the climate across the British Isles is likely to have fluctuated between

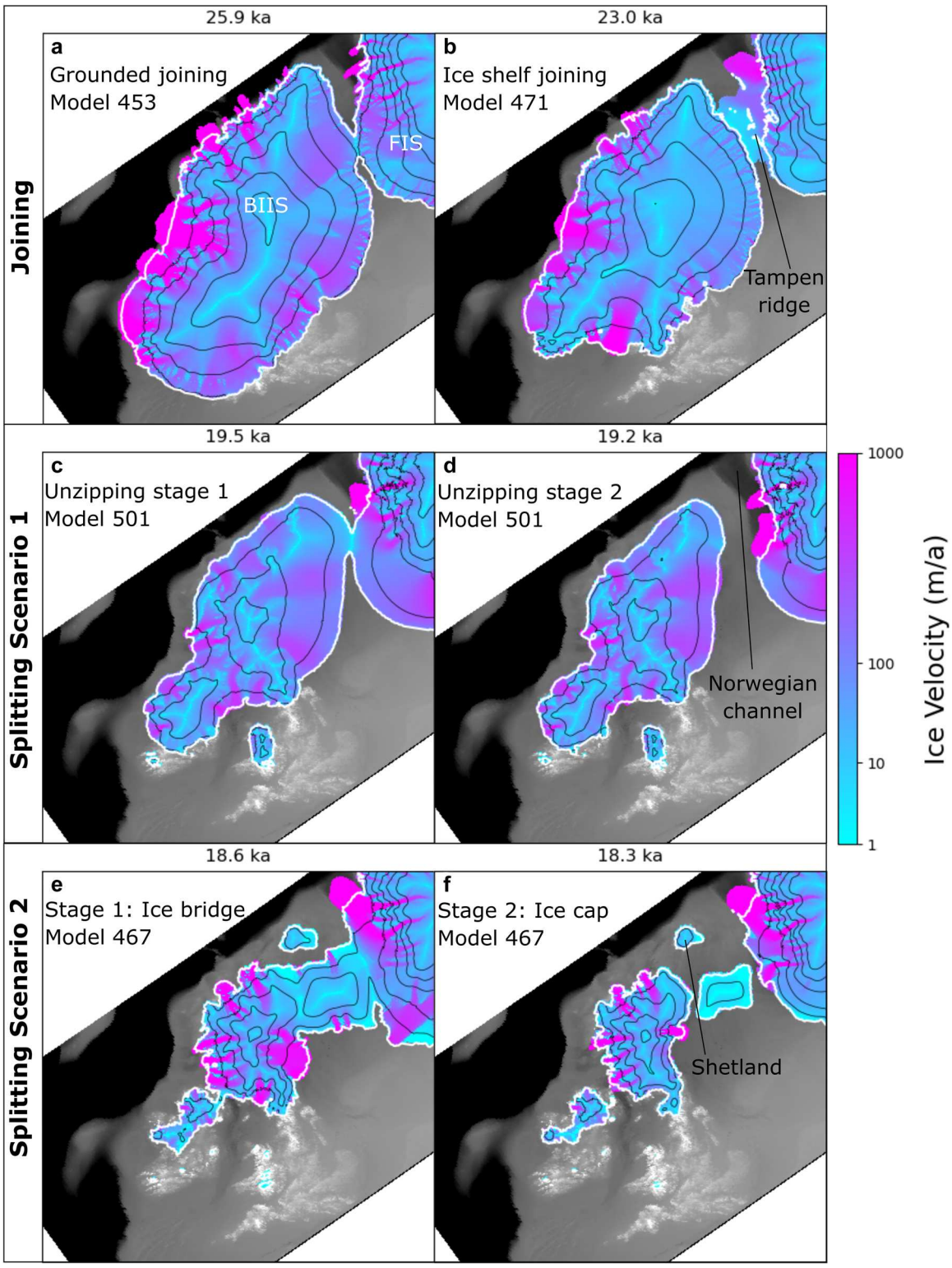

Figure 17. Common behaviour of the model in the North Sea. Joining of the British–Irish and Fennoscandian Ice Sheets occurs either when two grounded ice sheets touch (a), or when ice shelves meet, thicken and ground (b). Splitting of the two ice sheets often occurs by unzipping (c) and (d), as ice retreats along the Norwegian Channel Ice Stream and in the southern North Sea. Alternatively, the model sometimes produces an ice bridge between the two ice sheets (e), with a remnant ice cap in the North Sea left behind in some simulations (f). The black lines are 500 m elevation contours, and the white line is the edge of grounded ice. [Color figure can be viewed at wileyonlinelibrary.com]

conditions conducive for full glaciation, marginal glaciation and glacier-free states (Barr et al., 2019). Thus, small glaciers or ice caps, which are below the resolution of our model, probably existed at 32 ka BP. However, the order of magnitude difference in scale between mountain glaciers and ice sheets is a longstanding problem for modelling palaeo-ice sheet inception (Barry et al., 1975; Marshall and Clarke, 1999). This initial 1 ka period can therefore be seen as a spin-up of the model, with the rapid growth of ice probably a consequence of the modelled ice extent equilibrating with the prescribed climate. At 31 ka, our NROYs simulate a substantial ice cap over the highlands of Scotland, with smaller ice caps centred around other high ground such as in north-west Ireland, the Lake District and the Southern Uplands. The modelled ice is not extensive or thick enough during this time to produce marine-based ice. This ice extent is broadly consistent with limiting dates at Tolsta Head on the Isle of Lewis (Whittington

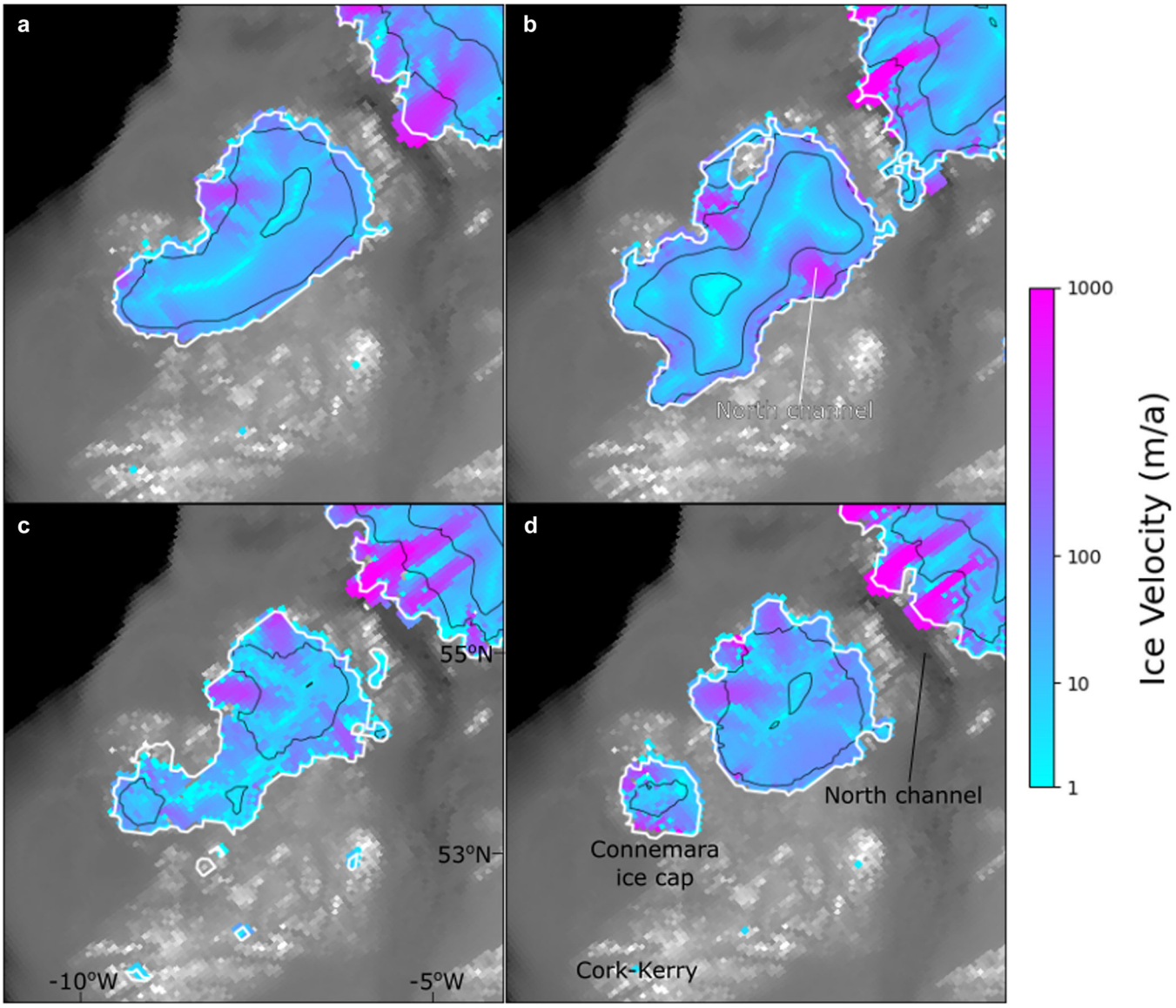

Figure 18. Modes of behaviour of the Irish Ice Sheet during deglaciation. (a) A single dome and ice divide. (b) A dual dome, with a more complex ice divide structure. (c) Tri-dome mode of behaviour, with the most complex divide structure. (d) Separate ice caps. Note that within a single model run, different modes of behaviour can occur through time. [Color figure can be viewed at wileyonlinelibrary.com]

and Hall, 2002) and south of the Scottish Highlands (Brown et al., 2007; Jacobi et al., 2009). Thus, despite an ice-free initial state, the 31 ka ice caps are broadly consistent with the evidence.

After 31 ka BP the ice sheet continues to rapidly grow, nucleating from several ice caps. Consistent with the reconstruction of Clark et al. (2022) the ice volume during this period rapidly increases (Figure 15), probably due to ice-positive feedback when ice caps merge. Ice elevation rapidly increases in the coalescence zone, e.g. between the Scottish and Irish Ice Sheets, increasing the overall mass balance. Furthermore, the ice margin perimeters reduce during mergers, meaning there is less space through which outlet glaciers can discharge ice. The largest collision between ice masses early in glaciation occurs between Scottish- and Irish-sourced ice over the North Channel region. Before collision, ice flow of both ice caps in the region occurs mostly via sheet flow. After collision, two ice streams form; a consequence of the reduced margin area through which ice can be output.

On a larger scale, 'saddle merger' events between ice sheets have been invoked to explain rapid sea-level drops during glaciations (Ji et al., 2021). Here we propose that the smaller scale saddle mergers of the BIIS played an important role in explaining both the surprisingly rapid glaciation and in driving the asynchronous maximum extents around the ice sheet. Such saddle merging events may be relevant to many other ice sheets and the process of glaciation inception in general. The biggest contrast in the timing of maximum extent is between the north-west of Scotland (30 ka, Bradwell et al., 2021) and east of England (22 ka, Evans et al., 2021). In Scotland, ice can rapidly expand to the neighbouring continental shelf due to neighbouring high ground accommodating ice caps which merge. However, it is not until the saddle merger between the FIS and BIIS occurs across the North Sea, that the maximum extent across the east of England occurs. Thus, saddle mergers interact with the placement of high ground to produce asynchronous ice maximums. Furthermore, this suggests that ice cover along the east coast of England requires a conjoining between the BIIS and FIS; an argument against a large early BIIS across the North Sea (e.g. Murton, 2021).

Since the changes induced by saddle merger, and indeed saddle collapse (Gregoire et al., 2012) are rapid, the topography essentially preconditions the BIIS to four states, summarised in Figure 20: (i) ice caps over high ground prior to saddle merging (Figure 20a); (ii) an independent British–Irish Ice Sheet, prior to saddle merging with the FIS (Figure 20b); (iii) a conjoined BIIS and FIS (Figure 20c); (iv) saddle collapse across the North Sea

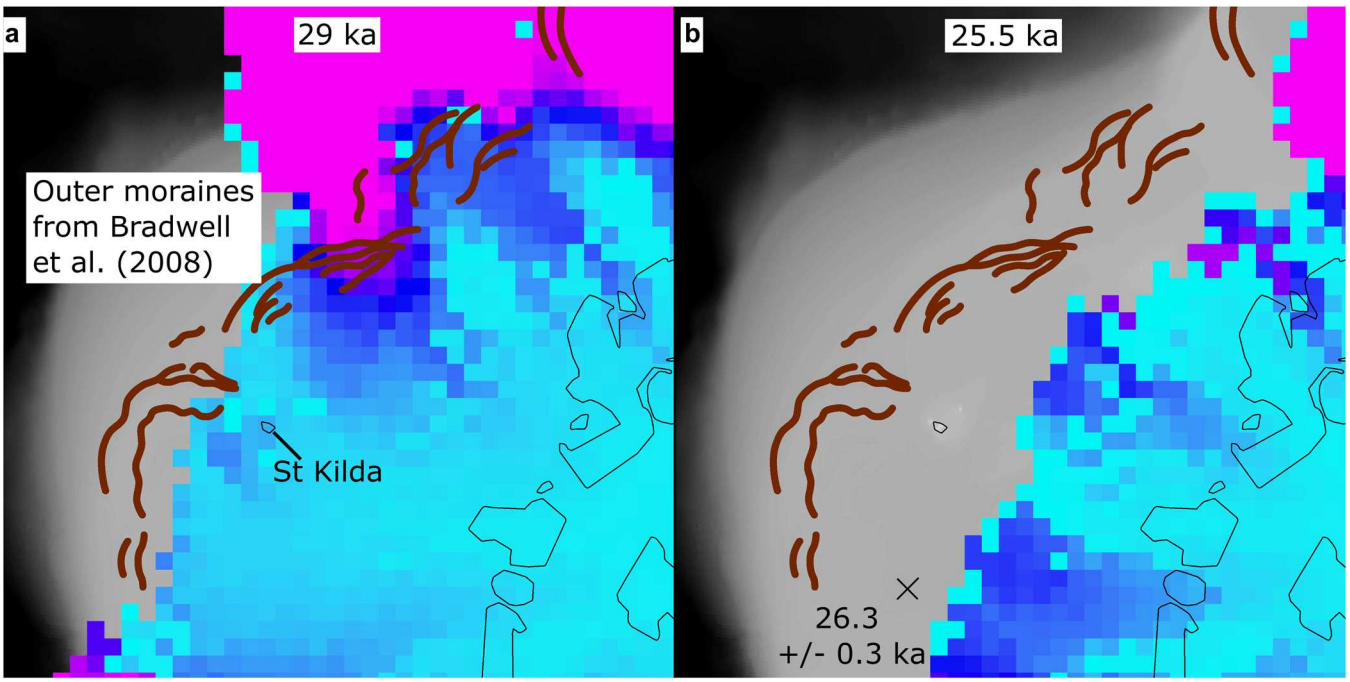

Figure 19. Model results west of the Hebrides near St Kilda. NROY experiment 488 is shown as illustrative of general model behaviour. (a) Ice streams and moraines at maximum. (b) Radiocarbon date from Peacock et al. (1992). [Color figure can be viewed at wileyonlinelibrary.com]

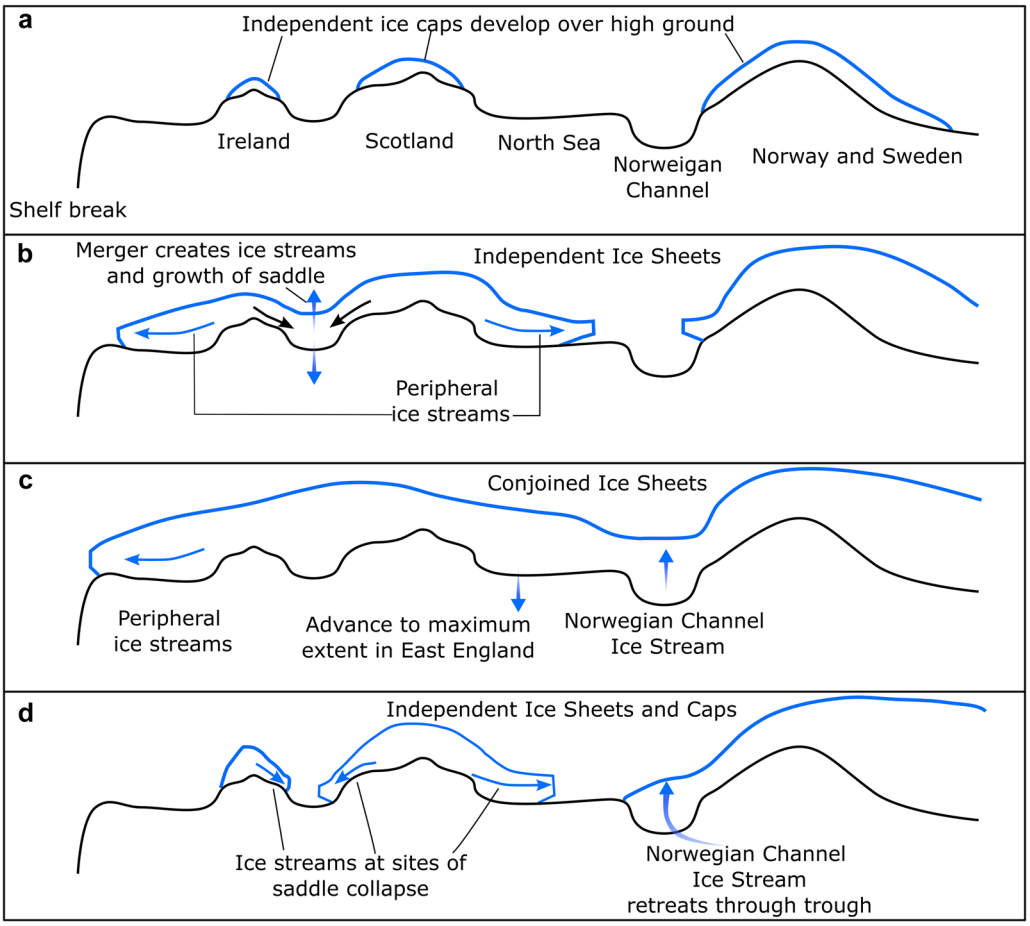

Figure 20. The impact of saddle merger and collapse events on the BIIS during ice-sheet growth and retreat. The topography interacts with ice map growth to precondition the BIIS to four common states, described further in the text. Ice caps initiate over high ground (a). Growth of these ice caps causes them to merge, reducing ice perimeter, causing ice streams and saddle growth. When the BIIS and FIS meet, the same process leads to the growth over a saddle over the North Sea, and the extension of the ice sheet along the east coast of England (c). During deglaciation, saddle collapse triggers ice streaming, and retreat to ice cap configurations (d). [Color figure can be viewed at wileyonlinelibrary.com]

and between ice caps leads to a state similar to that in Figure 20a, the difference being more rapid ice streams occurring during deglaciation due to ice–surface feedback (Figure 20d; Robel and Tziperman, 2016). Fluctuations between these states may reflect a local ice response to forcings.

Persistent model–data mismatch along marine margins

Several aspects of the marine-terminating portions of the BIIS proved difficult to simulate with the numerical model, creating two persistent model–data mismatches. The largest discrepancy between our model simulations and the reconstructed ice extent, is in the model's inability to reach the extremities of the BIIS in the Celtic Sea (Praeg et al., 2015; Scourse et al., 2019) and the Porcupine Bank (Peters et al., 2015; Ó Cofaigh et al., 2021). A second mismatch is in the inability of the model to produce the early retreat of marine-based ice in The Minch, Donegal Bay and Malin–Hebrides sectors (Bradwell et al., 2021b; Benetti et al., 2021; Ó Cofaigh et al., 2021). Such mismatches point either to a need for model improvement, improved realism of climate and ocean forcings or, in extreme circumstances, a re-evaluation of the underlying data (Ely et al., 2019).

Glaciogenic sediments indicate the most southerly extent of the BIIS as being the shelf edge in the Celtic Sea (Praeg et al., 2015), previously thought to be the Isles of Scilly (Scourse et al., 1990; Smedley et al., 2017). These glaciogenic sediments are thought to have been emplaced by an extension of the Irish Sea Ice Stream (Scourse et al., 2019), the extent of which has been inferred from seismic studies (Lockhart et al., 2018). This southerly maximum extent has been dated to approximately 25.5 ka BP, and probably occurred for a brief period of time before a rapid northerly retreat (Scourse et al., 2021). None of our NROY simulations reach the dated sites close to the continental shelf break, and though some simulations from the wider ensemble cover this region in ice, none match the timing of retreat (Figures 13 and 14). In the simulation which reaches the furthest south in the Celtic Sea, an ice extent for which there is currently no evidence occurs over south-west England (Cornwall and Devon), with ice advanced over the present-day coastline. In some non-NROY simulations, more extensive ice cover over south-west England occurs. In our opinion, the most likely cause for this mismatch relates to the difficulty of correctly simulating the dynamics of this short-lived extension of the BIIS, which has been hypothesised to relate to a surge event (Scourse and Furze, 2001; Scourse et al., 2021). Though PISM is capable of capturing surge-type behaviour (Van Pelt and Oerlemans, 2012), correctly simulating the timing and placement of these is challenging. The thermal regime of the ice sheet, dependent upon the climate forcing, must be correct to get surge behaviour in the right location and time. In common with our own simulations no ice-sheet model has been able to recreate the extent of the Irish Sea Ice Stream without incorrectly glaciating adjacent areas.

Geomorphological and geochronological evidence, in the form of a series of moraine ridges and radiocarbon dates constraining ice advance have been interpreted as evidence for an ice shelf grounding on the Porcupine Bank west of Ireland (Peters et al., 2015; Ó Cofaigh et al., 2021). Despite these constraints forming part of our model–data comparison routine, disappointingly, none of our NROYs recreated this westernmost extension of the BIIS (Figure 13). From an examination of all the simulations, rather than just those deemed NROY, we note that of the 400 simulations run at 10 km, only 11 managed to glaciate Porcupine Bank. These 11 simulations produced unrealistically thick ice sheets. A potential avenue for future work is to explore models that can deliver enough ice to the west coast of Ireland to ground on Porcupine Bank, without producing unrealistic ice thicknesses. This might require modelling which resolves higher bathymetry on Porcupine Bank, or an adaptation of the simulated relative sea level of the region, so that an advancing ice shelf is able to ground and then thicken. Furthermore, this rare example of a well-constrained palaeo-ice rise could be useful for understanding ice rises in general, especially given their importance in governing Antarctic Ice Sheet ice dynamics (Matsuoka et al., 2015).

A persistent model–data mismatch occurs along the continental shelf break west of Scotland and Ireland. Here, BRITICE-CHRONO found that retreat began much earlier than previously assumed, with some sectors commencing retreat as early as 30–27 ka BP (Ó Cofaigh et al., 2021; Clark et al., 2022). In general, our models perform poorly at recreating this early retreat (note the numerous crosses on Figure 13 in marine sectors). Indeed, some moraines in the Malin–Hebrides Sea never match an NROY simulation due to their inability to recreate the timing that these moraines were occupied (Figure 13). This was also challenging for the BRITICE-CHRONO reconstruction of Clark et al. (2022). We found that the models that performed comparatively well at matching deglaciation in marine sectors, were those with an ocean higher melt-rate parameter and increased calving rates. However, the likely cause of the overall poor match to data in marine sections is our simplistic, non-transient, ocean-forcing mechanism (see 'Climate forcing', above), which future work should seek to improve.

The persistent model–data mismatches in marine-terminating margins described above highlight the importance of ocean physics in governing ice-sheet evolution. Though this is becoming increasingly apparent in Antarctica (e.g. Reese et al., 2018), it appears that ice–ocean interactions were also important for the BIIS. Future work should explore more advanced means of capturing ice–ocean interactions, such as those explored by Petrini et al. (2020) or used to simulate the future of the Antarctic Ice Sheet (Reese et al., 2018), or data on ocean temperatures (El bani Altuna et al., 2021). However, constraining ocean temperature and salinity, which these more sophisticated ice–ocean models require, across palaeotimescales is challenging.

Location and persistence of ice streams and ice shelves

Ice streams occurred in our simulations throughout ice-sheet advance and decay. The simulated ice streams largely resemble those reported in the literature (Gandy et al., 2019), with the notable exception of the Celtic ice stream, the absence of which we discussed in the previous section. This correspondence between the model and observations is perhaps unsurprising, given that ice stream location was somewhat prescribed by inputting low till-friction values where ice streams have been reported ('Ice physics and PISM', above). Though this makes fast ice flow in such regions more likely, models could still create ice streams over other regions had conditions allowed (or fail to create an ice stream over low-friction areas).

The composite signature of ice streaming from all NROY simulations is shown in Figure 21 where the largest and most persistent ice streams were simulated in the marine sectors. Radiating inwards from these larger fast-flowing outlets are arborescent patterns of ice streams. These patterns arise by two mechanisms. First, many ice streams have tributary regions that

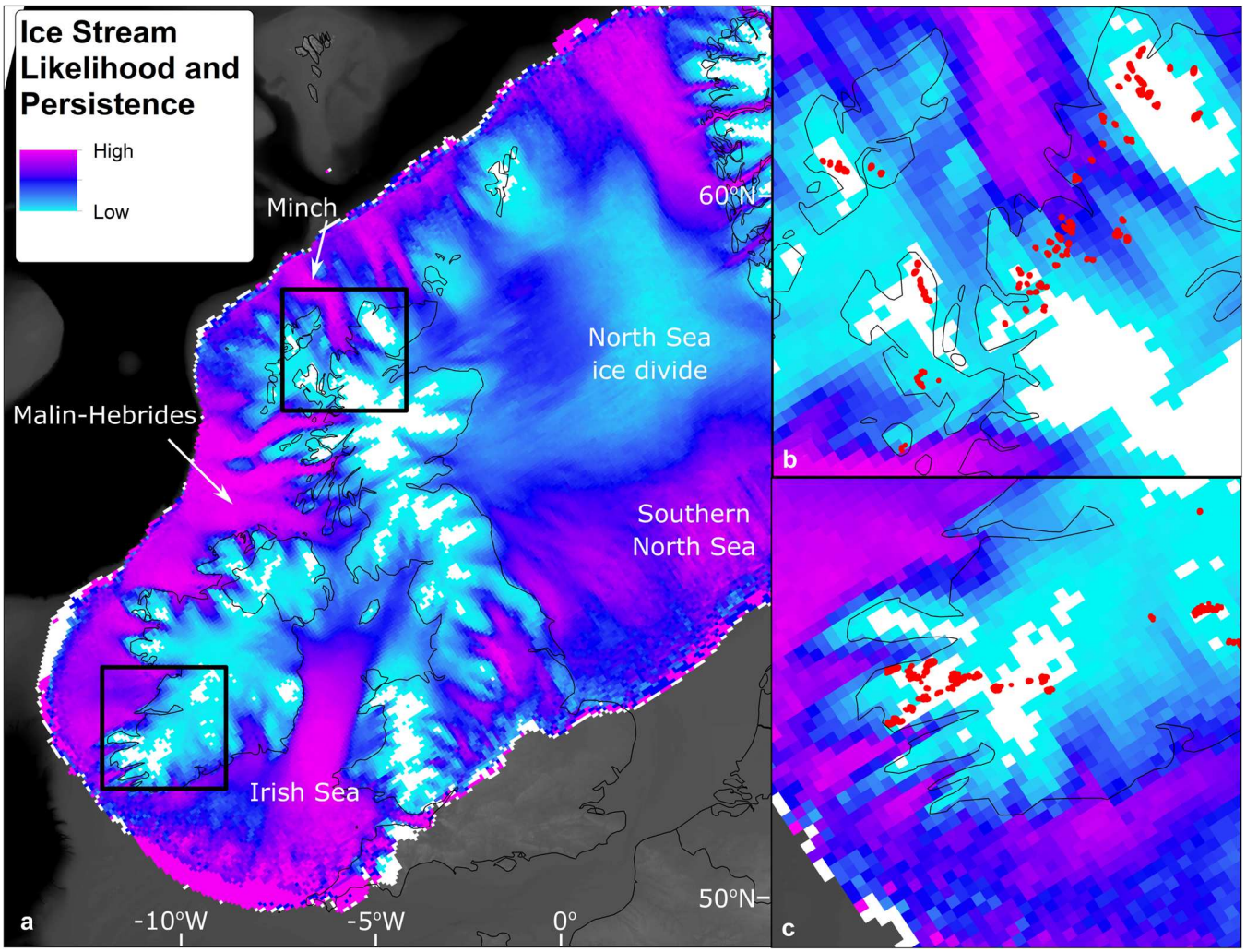

Figure 21. The location and persistence of fast flow. Fast flow was defined as regions of ice flowing above 100 m a^{-1}. Values reflect the number of NROY simulations (likelihood) that produce ice stream flow for over 100 years (persistence), once the differing durations of ice cover each NROY produces are accounted for. (a) Overall persistence of ice stream conditions map. (b) and (c) show the locations of trimlines (Clark et al., 2018) in relation to ice streams. Note how many are co-located with regions of low ice stream persistence and likelihood. Overall, this map could be viewed as a proxy for glaciation-scaled erosivity and compared with the distribution and type of landforms such as tors, roches moutonnées, U-shaped valleys, bedforms, etc. Modern-day coastline is shown for orientation. [Color figure can be viewed at wileyonlinelibrary.com]

feed them, in a similar manner to contemporary Antarctic and palaeo-Laurentide ice streams (Margold et al., 2015). Second, as deglaciation occurs, ice streaming tends to propagate upstream and inward of the main ice stream trunk. At many of the innermost regions of the ice sheet, ice streams were not created at any point by our NROY simulations, displayed white in the fast-flow persistence and likelihood map (Figure 21). These areas of zero to low ice stream likelihood show a striking correspondence with the locations of trimlines (as compiled by Clark et al., 2018; Figure 21), suggesting that it may be useful to quantify erosion rates in future work (e.g. Patton et al., 2022).

The most uncertain area of ice streaming occurs over the southern North Sea (e.g. Figures 16 and 21). Here, models tend to produce a broad region of fast flow, rather than a specific corridor of fast flow typical of modern ice streams. This is probably due to a lack of topographic focussing of the ice to concentrate an ice stream into a specific region (e.g. Winsborrow et al., 2010) and incomplete model physics to segment (into corridors) fast flow and organise into preferred spacings (e.g. Hindmarsh, 2009; Kyrke-Smith et al., 2015). A potential future modelling experiment could examine the role that a large ice-dammed glacial lake in the southern North Sea (e.g. Clark et al., 2012) may have had on the initiation and pattern of ice streaming. However, to directly tackle the palaeoglaciology of this area, further observations are required. This is challenging, as in the central North Sea, the models produced a distinct ice divide under which it is typical for very little landform production or sediment transport to occur, and so this area might always tend towards a blank on the map.

Ice shelves also occur throughout all our experiments. The persistence and likelihood of ice shelves from our NROY experiments are shown in Figure 22. The region with the highest likelihood for ice shelves is along the continental shelf break west of Scotland and Ireland (Figure 22). The only known evidence for an ice shelf here occurs in the Porcupine region (discussed in the previous section). Elsewhere on the west coasts, ice shelves are regularly simulated stretching into the deep ocean (Figure 22) but empirical evidence for their existence is yet to be found. However, the high tidal amplitudes around the BIIS during the last glacial (Scourse et al., 2018), a factor not considered by our ice-sheet model, may have prohibited ice shelf growth in the region. Thus, the more likely candidates for ice shelves would be those located closer to the modern-day coastlines where physical buttressing in bays and headlands promote ice shelf stability. This is especially the case in topographically confined regions,

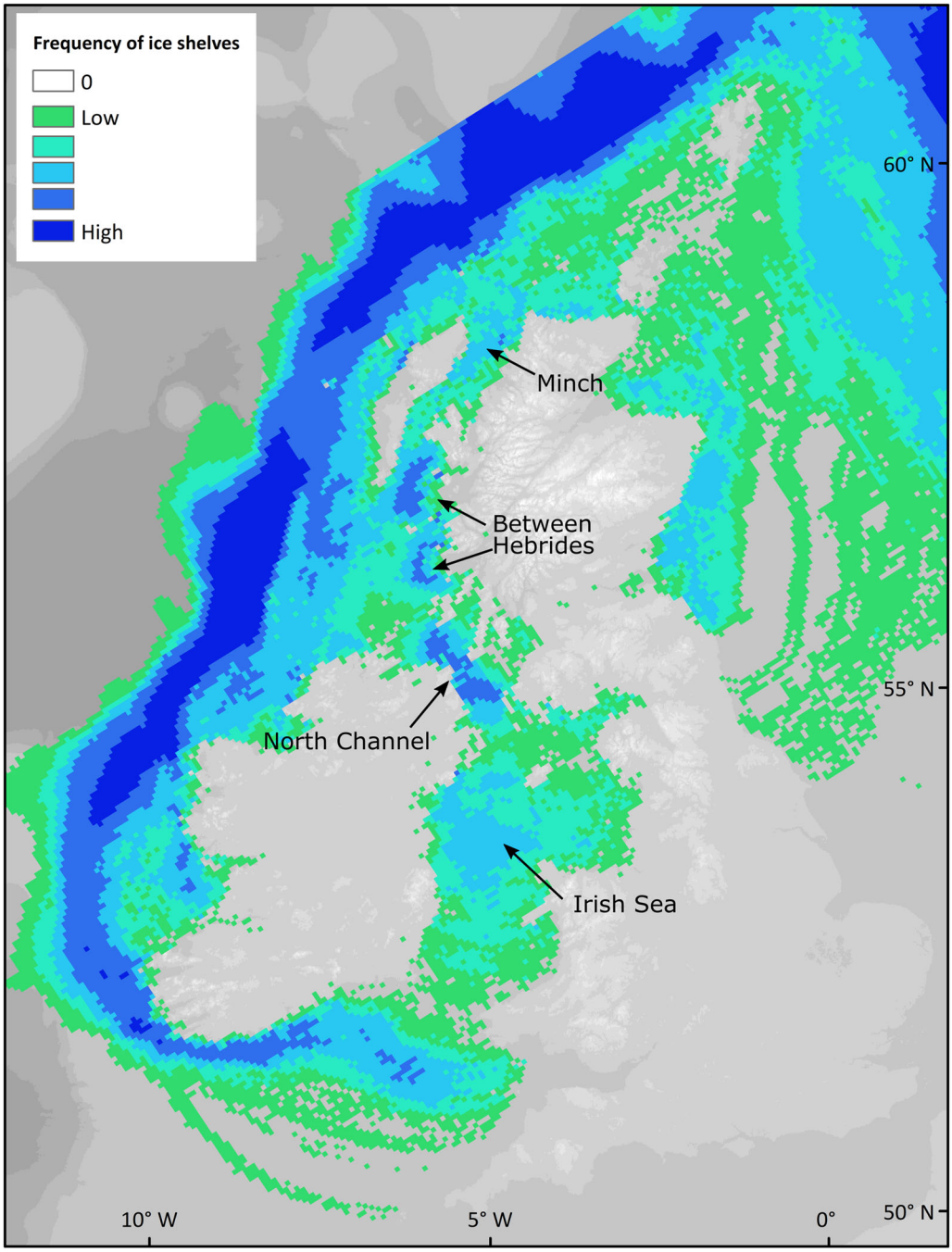

Figure 22. The predicted likely location of ice shelves from our NROY experiments. Note that shelves extending into the Atlantic may be unrealistic due to tidal forcing from mega-tides (Scourse et al., 2018). Potential ice shelf locations mentioned in the text are labelled and may be promising sites for future empirical work confirming or refuting ice shelf occurrence. [Color figure can be viewed at wileyonlinelibrary.com]

such as the North Channel, within the Irish Sea, and between the Inner and Outer Hebrides (Figure 22). Of most note is The Minch (between mainland Scotland and the Outer Hebrides) where seafloor evidence of flat-topped grounding zone wedges demonstrates that a large ice shelf existed and probably mediated ice retreat (Bradwell et al., 2021b). Modelling investigations of this Minch Ice Stream by Gandy et al. (2018) pointed to the role of the modelled ice shelf in buttressing ice stream flow. Most of the modelled ice shelves in our NROY simulations await further investigation; that they regularly occur in model runs that most closely match the empirical data regarding the deglaciation of the BIIS suggests that Figure 22 could serve as a useful map for targeted empirical work to find possible sedimentological records of ice shelf presence (e.g. Smith et al., 2023).

Readvances

The rich geomorphological and sedimentological record of the BIIS has been interpreted to record multiple ice marginal readvances (e.g. Catt and Penny, 1966; McCabe et al., 2007; Bradwell et al., 2021a; Roberts et al., 2019; Table 8). For our purposes, a readvance is defined as the regrowth of an ice sheet over an area following recent retreat. We conducted a literature review which revealed that 17 such readvances of the BIIS have been postulated in the literature, during our modelled time period (Table 8). Though the exact mechanisms behind these readvances are debated, they have often been attributed to either specific climatic cooling events (e.g. Ballantyne et al., 2009; McCabe et al., 2007) or by internal glaciologically driven oscillations of the ice sheet (e.g. Bradwell et al., 2008).

Table 8. Reported readvances of the BIIS during our modelled time frame

Location	Evidence	Approximate timing (ka BP)	References
Continental shelf north of Shetland	Scalloped morphology of the Greenwich Meridian Readvance Moraine and radiocarbon dating of material within glacial diamict.	21.6	Bradwell et al., 2021a; Ross, 1996
Eastern England (Skipsea, Little Catwick/Gembling, Sandsend/ Ferrybridge)	Retreat and readvance sequences within the Skipsea Till and similar Catwick/Gembling stratigraphy.	23.5	Evans and Thomson (2010); Bateman et al., 2018; Roberts et al., 2019)
East coast of England (Dimlington, Withernsea, Holderness)	Oscillatory ice margin recorded by interbedded sequences of tills and ice-contact lake deposits.	21.5	Catt and Penny, 1966; Rose, 1985; Evans and Thomson, 2010
North Sea Lobe, offshore eastern England	Radiocarbon dating from laminated sediments below a glacial diamict. Thought to be triggered by a switch from terrestrial to marine conditions. Timing supported by onshore dates and wider deglacial context.	19.5	Roberts et al., 2019
Welsh ice cap	Ice sheet modelling experiments and offshore glacial geomorphology in Cardigan Bay suggest readvances of outlet glaciers. Eastern and northern outlet glaciers potentially also readvanced. Thought to be triggered by the retreat of neighbouring glaciers.	21.1	Patton et al., 2013; Evans et al., 2005; Chiverrell et al., 2021
Celtic Sea	Deformed glaciomarine muds. Status as full readvance or adjustment of grounded margin unknown.	25.5	Lockhart, 2020; Scourse et al., 2021
Between south-east Ireland and south-west Wales	Coincides with narrowing of Irish Sea Ice Stream channel. Likely minor.	24.5	Ó Cofaigh and Evans, 2007; Scourse et al., 2021
Scottish readvance, potentially extending across the Isle of Man and Cumbrian lowlands	Thin till within the Solway Lowlands, glaciotectonised sediments within moraines. Likely >10 km of retreat and advance.	20 +/−0.4 18.9 +/−1.1	Trotter et al., 1937; Chiverrell et al., 2018; Scourse et al., 2021; Livingstone et al., 2010; Williams et al., 2001
Isle of Man	Small (km-scale) readvances recorded in sediment sequences.	19.3 +/−0.8	Thomas et al., 2004; Chiverrell et al., 2018
Killard Point (north-east Ireland)	Radiocarbon dating bracketing a readvance.	17.4 +/−0.3	Chiverrell et al., 2018; McCabe et al., 2007
Clogher Head (north-east Ireland)	Radiocarbon dating bracketing a readvance.	18.7 +/−0.2	Chiverrell et al., 2018; McCabe et al., 2007
Porcupine Bank	Reworked shells within tills and overridden glaciomarine sediments. Indicate fluctuations in grounding on Porcupine Bank.	25.9 +/−1.8 to 25.4 +/−0.25	Ó Cofaigh et al., 2021
Galway Bay	Oscillating grounding line, recorded in seismic data. A series of grounding zone wedges and smaller moraines. Deformed deglacial sediments.	25.0 +/−0.35	Callard et al., 2020; Peters et al., 2016
Killala Bay	Moraines that overprint prior deglacial moraines.	20.5 to 19.0.	Ó Cofaigh et al., 2012; Wilson et al., 2019; Benetti et al., 2021
Corvish, Donegal Ireland	Radiocarbon dating of glaciotectonised sediments.	19.5 to 18.3	McCabe and Clark, 2003; Wilson et al., 2019
Wester Ross	Demarked by a series of moraines, with erratics inferred to correspond to a readvance. Cosmogenic nuclide dating.	15.3 +/−0.7	Robinson and Ballantyne, 1979; Ballantyne et al., 2009; Ballantyne and Small, 2019
East Minch	Cross-cutting moraines. DeGeer moraines which overly larger moraines.	21.4 to 19.0	Bradwell et al., 2021b

Empirical evidence of such events is often restricted to point-sourced data (e.g. a single stratigraphic section spanning just hundreds of metres). Thus, determining the spatial extent of a readvance is difficult; by how many kilometres did the margin retreat before readvancing? This is important for building and assessing the wider significance of such oscillations in palaeoreconstructions. Numerical modelling simulations may help fill such gaps in knowledge. Furthermore, when robustly found, readvances can be used to assess the sensitivity of the BIIS to either external or internal fluctuations.

To assess whether readvances were reproduced by our NROY simulations, we examined each simulation against those defined empirically in Table 8 noting the relevant time periods and locations with the requirement for ice-free conditions to be followed by a readvance. Due to insufficient simulated ice extent our models could not achieve the readvances of the Celtic Sea break (Scourse et al., 2021) and Porcupine Bank (Ó Cofaigh et al., 2021), and did not match well with the Wester Ross readvance (Ballantyne and Small, 2019) due to the temporal constraints of our model. Qualitatively, we found that many of the readvances of Table 8 were replicated in our model. However, the scale of simulated readvances was often small, limited to oscillations of the margin which were in the order of ~20–50 km in scale. Furthermore, readvances tended to be localised to specific regions of the ice sheet, as small fluctuations during overall retreat, rather than synchronous large margin changes across

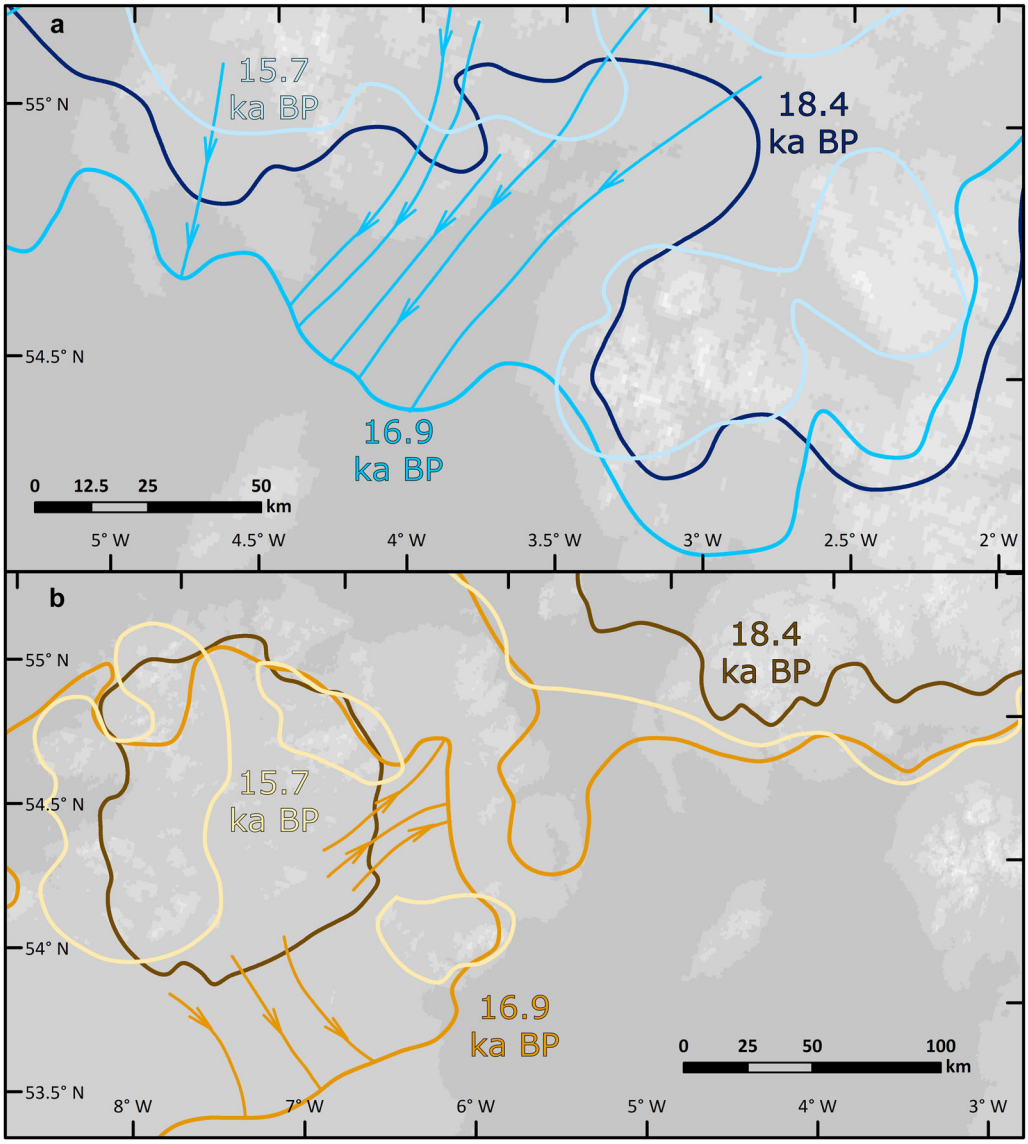

Figure 23. Examples of readvances simulated by our NROY experiments. Flowlines of the major outlet glaciers simulated by the model during readvance are denoted by arrows. Note that these are imperfect model simulations. As such, we do not expect these isochrones to perfectly match the timing or position of reconstructed readvances. Rather, they are illustrative of the types of readvance behaviour replicated by the model. For both readvances shown, the Scottish (a) and those which occurred on the east coast of Ireland (b), the distance over which the ice sheet readvances is in the order of 50 km and is often localised to a specific margin. In the case of the simulated Scottish readvance (a), the model probably overshoots the distance of the readvance, which is thought to be sourced solely from Scottish ice (Livingstone et al., 2010). In north-east Ireland (b), this simulation roughly covers the areas of Killard point and Clougher head (Table 8). [Color figure can be viewed at wileyonlinelibrary.com]

the entirety of the ice sheet. Examples of such are shown in Figure 23. This suggests that in some cases the readvances are not purely a consequence of climate cooling episodes (e.g. Heinrich events), occurring only at specific locations rather than producing the ice-sheet wide response expected from a cooling or increase in precipitation.

A previous set of modelling experiments of the BIIS, produced a dynamic and rapidly fluctuating ice sheet that produced large readvances over several hundreds of kilometres (Hubbard et al., 2009). The cause of these readvances was thermomechanical coupling leading to binge–purge cycles (Hubbard et al., 2009). In contrast, our models of the BIIS have fewer, more subdued and localised readvances (e.g. Figure 23). Accurately determining the cause of this difference in model behaviour would require a model intercomparison exercise, whereby both models were forced with similar boundary conditions. In the absence of such an activity, we suggest that the likely candidate for this divergence in model behaviour is their different treatment of the subglacial environment. In the Hubbard et al. (2009) model, sliding occurs once pressure melting is reached. Beyond this, water is not accounted for. Our simulations, though simplistic in their treatment of water ('Ice physics and PISM', above), buffer this thermomechanical feedback on sliding by storing water in a subglacial till later. In contrast to the Hubbard et al. (2009) model, ice streams are less dynamic and perhaps our treatment of water acts to stabilise ice stream position, dampening the thermomechanical feedback associated with binge–purge behaviour (e.g. MacAyeal, 1993). An alternative is that the binge–purge behaviour is dampened in our simulations by the forcing factor that we apply. However, ice temperature variations are not changed by the forcing factor, and simulations with a low forcing value also fail to display binge–purge-like behaviour.

In our interpretation, the readvances we observe are neither a simple response to climate forcing (due to their limited spatial scale), nor caused by thermomechanical internal

feedback. Though it is likely that different processes act at different locations to produce a readvance, this causes us to postulate on a further trigger. We note that many of the readvances we observe occur in the spatial and temporal vicinity of ice mass separation. For example, the Kilkeel readvance and Scottish readvance occur near to the suture zone between Scotland and Ireland. Thus, our interpretation is that some readvances may be triggered by an internal reorganisation of the ice after separation from a neighbouring ice mass, though this idea requires future investigation, perhaps utilising idealised ice-sheet geometries. Future work should isolate the causes of readvances, considering the potential internal and external triggers discussed here, and we suggest caution is exercised in using empirically defined localised readvances to infer major climate events.

Persistence of peripheral ice caps

Despite lying beyond the constrained boundary of the ice sheet, and thus discouraged by our climate forcing ('Climate forcing', above), two large peripheral ice caps often develop in our modelling experiments. Evidence for the first, the Dartmoor ice cap, has previously been examined (Evans et al., 2012), though an empirical constraint on the timing of the existence of this ice cap is currently lacking. Our model most frequently glaciates this region during the early stages of glaciation (~30 ka), and the existence of a Dartmoor ice cap is often limited in timespan to a few hundred years. This is consistent with the weakly developed glacial landscape and landforms of the Dartmoor region (Evans et al., 2012). A second ice cap also frequently appears in the Peak District. Evidence of glaciation in this region is piecemeal, and often attributed to previous glacial stages or small-scale cirque-like glaciation (Johnson et al., 1990; Burek, 1991), though there is a distinct lack of dated material. The simulation of a Peak District ice cap is either a model error, or a line of enquiry warranting further work. The model also predicts numerous smaller regions of ice cover peripheral to the main ice sheet. The small size of these (generally less than four grid cells) is probably beyond the resolution of the model.

Outlook and conclusions

An integration between numerical models and empirical data has been a long-term goal of the palaeoglaciological community (Andrews, 1982). The proliferation of ice-sheet models, increased access to relevant computing resources, and the ongoing development of model–data comparison tools means that progress towards this goal should accelerate. As tighter model–data integration occurs, we hope this study highlights a pathway for model–data comparison that can provide a means of integrating numerical modellers and Quaternary scientists. Progress in ice-sheet reconstruction has been made through expert-driven reconstructions that attempt to satisfy as much of the available data as possible (e.g. Clark et al., 2012) – models now provide a physics-based approach for recreating this process (e.g. Clark et al., 2022) to build model reconstructions or data-calibrated models. As we have conducted here, this means that like their empirical counterparts, ice-sheet models can be used to test and generate hypotheses of palaeo-ice-sheet behaviour. Essential to this process is the quantification of model–data misfit, which will inevitably require further improvements to model–data comparison tools. Given the uncertainty in climatic and ocean forcings, the limitations of computer resources, plus the shortcomings of ice-sheet models, it is unlikely that a single model will capture all aspects of the BIIS data in the near future. In future work, difficult data for modellers to fit should be highlighted, as either a future target for model improvement, or as a means of highlighting potential data outliers that need re-examining.

As the most densely constrained palaeo-ice sheet, the BIIS is an ideal testing ground for model–data comparison experiments. Through an ensemble approach and data model comparison, the models that best fit aspects of the data were identified. No single model was able to replicate every aspect of the data, highlighting the need for multiple simulations to be conducted. Persistent model–data mismatch occurred mostly in marine-terminating sectors, demonstrating that an improved implementation of ice–ocean coupling is required. Particular regions that stand out for future work are the potential ice rise that formed on the Porcupine Bank, and the southerly extension of the Celtic Sea Ice Stream. Despite mismatches, we were able to capture the broad characteristics of the BIIS and its dynamics over time. This included aspects of the ice sheet's flow geometry, margin shape and retreat rates. This processing of identifying models which captured the data allowed us to explore a range of possible behavioural dynamics for which little to no data exist. Specifically, our models highlighted a range of possible behaviour in the North Sea, which demonstrates a high variability in model behaviour, attributable to different schemes for determining rates of basal sliding. The simulations show the dynamic behaviour of the ice sheet during growth and retreat, exhibiting numerous saddle mergers and collapses which contributed to ice-sheet growth and retreat. The result of these processes means that the modelled versions of the BIIS exhibited three common states, preconditioned by the geography of the British Isles: ice caps situated over high ground, an independent ice sheet and a larger part of the Eurasian ice-sheet complex. Furthermore, our models allow us to postulate on the possible locations of ice shelves, for which there is a lack of palaeodata, and the persistence of ice streams.

Overall, this work demonstrates how integrating numerical models and empirical data on ice-flow direction, margin shape and deglaciation timing, can elucidate both physically and empirically plausible ranges of palaeo-ice sheet behaviour. Moreover, we show that such interactions can produce advances for both Quaternary scientists and ice-sheet modellers.

Acknowledgements. This work was funded by the Natural Environment Research Council consortium grant BRITICE-CHRONO NE/J009768/1, and thanks are due for discussions with the numerous researchers on this project and notably, Richard Hindmarsh. JCE acknowledges support from a NERC independent fellowship award (NE/R014574/1). The project benefited from the PalGlac team of researchers with funding from the European Research Council under the European Union's Horizon 2020 research and innovation programme to CDC (Grant agreement No. 787263) and which supported SB and RA. For the purpose of open access, the author has applied a Creative Commons Attribution (CC BY) licence to any Author Accepted Manuscript version of this paper arising from this submission.

Data availability statement

The data that support the findings of this study are available from the corresponding author upon reasonable request.

Supporting information

Additional supporting information can be found in the online version of this article.

Abbreviations. AFDA, Automated Flow Direction Analysis; APCA, Automated Proximity and Conformity Analysis; ATAT, Automated

Timing Accordance Tool; BIIS, British–Irish Ice Sheet; EPICA, European Project for Ice Coring in Antarctica; FIS, Fennoscandian Ice Sheet; GIA, glacio-isostatic adjustment; GRIP, Greenland Ice Core Project; NCIS, Norwegian Channel Ice Stream; NROY, not ruled out yet; PDD, positive degree-day; PISM, Parallel Ice Sheet Model; PMIP3, Paleoclimate Modelling Intercomparison Project Phase III; SIA, shallow ice approximation; SSA, shallow shelf approximation; wRMSE, weighted root mean squared error.

References

Albrecht, T., Martin, M., Haseloff, M., Winkelmann, R. & Levermann, A. (2011) Parameterization for subgrid-scale motion of ice-shelf calving fronts. *The Cryosphere*, 5, 35–44.

Albrecht, T., Winkelmann, R. & Levermann, A. (2020) Glacial-cycle simulations of the Antarctic Ice Sheet with the Parallel Ice Sheet Model (PISM)–Part 2: parameter ensemble analysis. *The Cryosphere*, 14, 633–656.

Andrews, J.T. (1982) On the reconstruction of Pleistocene ice sheets: A review. *Quaternary Science Reviews*, 1, 1–30.

Aschwanden, A., Aðalgeirsdóttir, G. & Khroulev, C. (2013) Hindcasting to measure ice sheet model sensitivity to initial states. *The Cryosphere*, 7, 1083–1093.

Aschwanden, A. & Blatter, H. (2009) Mathematical modeling and numerical simulation of polythermal glaciers. *Journal of Geophysical Research: Earth Surface*, 114(F1), F01027. Available from: https://doi.org/10.1029/2008JF001028

Aschwanden, A., Bueler, E., Khroulev, C. & Blatter, H. (2012) An enthalpy formulation for glaciers and ice sheets. *Journal of Glaciology*, 58, 441–457.

Ballantyne, C.K., Fabel, D., Gheorghiu, D., Rodés, Á., Shanks, R. & Xu, S. (2017) Late Quaternary glaciation in the Hebrides sector of the continental shelf: cosmogenic nuclide dating of glacial events on the St Kilda archipelago. *Boreas*, 46, 605–621.

Ballantyne, C.K., Schnabel, C. & Xu, S. (2009) Readvance of the last British–Irish ice sheet during Greenland interstade 1 (GI-1): the Wester Ross readvance, NW Scotland. *Quaternary Science Reviews*, 28, 783–789.

Ballantyne, C.K. & Small, D. (2019) The last Scottish ice sheet. *Earth and Environmental Science Transactions of the Royal Society of Edinburgh*, 110, 93–131.

Barr, I.D., Ely, J.C., Spagnolo, M., Spagnolo, M., Evans, I.S. & Tomkins, M.D. (2019) The dynamics of mountain erosion: cirque growth slows as landscapes age. *Earth Surface Processes and Landforms*, 44, 2628–2637.

Barry, R.G., Andrews, J.T. & Mahaffy, M.A. (1975) Continental ice sheets: conditions for growth. *Science*, 190, 979–981.

Barth, A.M., Clark, P.U., Clark, J., McCabe, A.M. & Caffee, M. (2016) Last Glacial Maximum cirque glaciation in Ireland and implications for reconstructions of the Irish Ice Sheet. *Quaternary Science Reviews*, 141, 85–93. Available from https://doi.org/10.1016/j.quascirev.2016.04.006

Bateman, M.D., Evans, D.J.A., Roberts, D.H., Medialdea, A., Ely, J. & Clark, C.D. (2018) The timing and consequences of the blockage of the Humber Gap by the last British—Irish Ice Sheet. *Boreas*, 47, 41–61.

Benetti, S., Chiverrell, R.C., Cofaigh, C.Ó., Burke, M., Medialdea, A., Small, D. et al. (2021) Exploring controls of the early and stepped deglaciation on the western margin of the British Irish Ice Sheet. *Journal of Quaternary Science*, 36, 833–870.

Boulton, G. & Hagdorn, M. (2006) Glaciology of the British Isles Ice Sheet during the last glacial cycle: form, flow, streams and lobes. *Quaternary Science Reviews*, 25, 3359–3390.

Boulton, G.S. & Clark, C.D. (1990) A highly mobile Laurentide ice sheet revealed by satellite images of glacial lineations. *Nature*, 346, 813–817.

Braconnot, P., Harrison, S.P., Kageyama, M., Bartlein, P.J., Masson-Delmotte, V., Abe-Ouchi, A. et al. (2012) Evaluation of climate models using palaeoclimatic data. *Nature Climate Change*, 2, 417–424.

Bradley, S.L., Ely, J.C., Clark, C.D., Edwards, R.J. & Shennan, I. (2023) Reconstruction of the palaeo-sea level of Britain and Ireland arising from empirical constraints of ice extent: implications for regional sea level forecasts and North American ice sheet volume. *Journal of Quaternary Science*, 38, 791–805.

Bradwell, T., Fabel, D., Clark, C.D., Chiverrell, R.C., Small, D., Smedley, R.K. et al. (2021b) Pattern, style and timing of British–Irish Ice Sheet advance and retreat over the last 45 000 years: evidence from NW Scotland and the adjacent continental shelf. *Journal of Quaternary Science*, 36, 871–933.

Bradwell, T., Small, D., Fabel, D., Clark, C.D., Chiverrell, R.C., Saher, M.H., et al. (2021a) Pattern, style and timing of British–Irish Ice Sheet retreat: Shetland and northern North Sea sector. *Journal of Quaternary Science*, 36, 681–722.

Bradwell, T. & Stoker, M.S. (2015) Submarine sediment and landform record of a palaeo-ice stream within the British–Irish Ice Sheet. *Boreas*, 44(2), 255–276. Available from https://doi.org/10.1111/bor.12111

Bradwell, T., Stoker, M. & Larter, R. (2007) Geomorphological signature and flow dynamics of The Minch palaeo-ice stream, northwest Scotland. *Journal of Quaternary Science*, 22, 609–617.

Bradwell, T., Stoker, M.S. (2015) Submarine sediment and landform record of a palaeo-ice stream within the British–Irish Ice Sheet. *Boreas*, 44, 255–276.

Bradwell, T., Stoker, M.S., Golledge, N.R., Wilson, C.K., Merritt, J.W., Long, D. et al. (2008) The northern sector of the last British Ice Sheet: maximum extent and demise. *Earth-Science Reviews*, 88, 207–226.

Briggs, R.D., Pollard, D. & Tarasov, L. (2014) A data-constrained large ensemble analysis of Antarctic evolution since the Eemian. *Quaternary Science Reviews*, 103, 91–115.

Briggs, R.D. & Tarasov, L. (2013) How to evaluate model-derived deglaciation chronologies: a case study using Antarctica. *Quaternary Science Reviews*, 63, 109–127.

Briner, J.P., Cuzzone, J.K., Badgeley, J.A., Young, N.E., Steig, E.J., Morlighem, M. et al. (2020) Rate of mass loss from the Greenland Ice Sheet will exceed Holocene values this century. *Nature*, 586, 70–74.

Brown, E.J., Rose, J., Coope, R.G. & Lowe, J.J. (2007) An MIS 3 age organic deposit from Balglass Burn, central Scotland: palaeoenvironmental significance and implications for the timing of the onset of the LGM ice sheet in the vicinity of the British Isles. *Journal of Quaternary Science*, 22, 295–308.

Bueler, E. & Brown, J. (2009) Shallow shelf approximation as a "sliding law" in a thermomechanically coupled ice sheet model. *Journal of Geophysical Research: Earth Surface*, 114, F3.

Bueler, E. & van Pelt, W. (2015) Mass-conserving subglacial hydrology in the Parallel Ice Sheet Model version 0.6. *Geoscientific Model Development*, 8, 1613–1635.

Burek, C.V. (1991) Quaternary history and glacial deposits of Peak district. In: Ehlers, J., Gibbard, P.L. & Rose, J. (Eds.) *Glacial deposits in Great Britain and Ireland*. Rotter-Dam: AA Balkema. pp. 193–201.

Callard, S.L., Ó Cofaigh, C., Benetti, S., Chiverrell, R.C., Van Landeghem, K.J.J., Saher, M.H. et al. (2020) Oscillating retreat of the last British-Irish Ice Sheet on the continental shelf offshore Galway Bay, western Ireland. *Marine Geology*, 420, 106087.

Calov, R. & Greve, R. (2005) A semi-analytical solution for the positive degree-day model with stochastic temperature variations. *Journal of Glaciology*, 51, 173–175.

Carr, S.J., Holmes, R., Van der Meer, J.J.M. & Rose, J. (2006) The Last Glacial Maximum in the North Sea Basin: micromorphological evidence of extensive glaciation. *Journal of Quaternary Science*, 21, 131–153.

Catt, J.A. & Penny, L.F. (1966) The Pleistocene deposits of holderness, east Yorkshire. *Proceedings of the Yorkshire Geological Society*, 35, 375–420.

Chiverrell, R.C., Smedley, R.K., Small, D., Ballantyne, C.K., Burke, M.J., Callard, S.L. et al. (2018) Ice margin oscillations during deglaciation of the northern Irish Sea Basin. *Journal of Quaternary Science*, 33, 739–762.

Chiverrell, R.C., Thomas, G.S.P., Burke, M., Medialdea, A., Smedley, R., Bateman, M. et al. (2020) The evolution of the terrestrial-terminating Irish Sea glacier during the last glaciation. *Journal of Quaternary Science*, 36(5), 752–779. Available at https://doi.org/10.1002/jqs.3229

Chiverrell, R.C., Thrasher, I.M., Thomas, G.S.P., Lang, A., Scourse, J.D., van Landeghem, K.J.J. et al. (2013) Bayesian modelling the retreat of the Irish Sea Ice Stream. *Journal of Quaternary Science*, 28, 200–209.

Clark, C.D., Chiverrell, R.C., Fabel, D., Hindmarsh, R.C.A., Ó Cofaigh, C. & Scourse, J.D. (2021) Timing, pace and controls on ice sheet retreat: an introduction to the BRITICE-CHRONO transect reconstructions of the British–Irish Ice Sheet. *Journal of Quaternary Science*, 36, 673–680.

Clark, C.D., Ely, J.C., Greenwood, S.L., Hughes, A.L.C., Meehan, R., Barr, I.D. et al. (2018) BRITICE Glacial Map, version 2: a map and GIS database of glacial landforms of the last British–Irish Ice Sheet. *Boreas*, 47, 11–e8.

Clark, C.D., Ely, J.C., Hindmarsh, R.C.A., Bradley, S., Ignéczi, A., Fabel, D. et al. (2022) Growth and retreat of the last British–Irish Ice Sheet, 31 000 to 15 000 years ago: the BRITICE-CHRONO reconstruction. *Boreas*, 51, 699–758.

Clark, C.D., Hughes, A.L.C., Greenwood, S.L., Jordan, C. & Sejrup, H.P. (2012) Pattern and timing of retreat of the last British-Irish Ice Sheet. *Quaternary Science Reviews*, 44, 112–146.

Dalton, A.S., Margold, M., Stokes, C.R., Tarasov, L., Dyke, A.S., Adams, R.S. et al. (2020) An updated radiocarbon-based ice margin chronology for the last deglaciation of the North American Ice Sheet Complex. *Quaternary Science Reviews*, 234, 106223.

Davies, B.J., Darvill, C.M., Lovell, H., Bendle, J.M., Dowdeswell, J.A., Fabel, D. et al. (2020) The evolution of the Patagonian Ice Sheet from 35 ka to the present day (PATICE). *Earth-Science Reviews*, 204, 103152.

DeConto, R.M. & Pollard, D. (2016) Contribution of Antarctica to past and future sea-level rise. *Nature*, 531, 591–597.

Dove, D., Arosio, R., Finlayson, A., Bradwell, T. & Howe, J.A. (2015) Submarine glacial landforms record Late Pleistocene ice-sheet dynamics, Inner Hebrides, Scotland. *Quaternary Science Reviews*, 123, 76–90.

Dunlop, P., Shannon, R., McCabe, M., Quinn, R. & Doyle, E. (2010) Marine geophysical evidence for ice sheet extension and recession on the Malin Shelf: New evidence for the western limits of the British Irish Ice Sheet. *Marine Geology*, 276, 86–99.

Dyke, A.S. (2004) An outline of North American deglaciation with emphasis on central and northern Canada. *Developments in Quaternary Sciences*, 2, 373–424.

El bani Altuna, N., Rasmussen, T.L., Ezat, M.M., et al. (2021) Deglacial bottom water warming intensified Arctic methane seepage in the NW Barents Sea. *Communications Earth & Environment*, 2, 188. Available from: https://www.nature.com/articles/s43247-021-00264-x

Ely, J.C., Clark, C.D., Hindmarsh, R.C.A., Hughes, A.L.C., Greenwood, S.L., Bradley, S.L. et al. (2021) Recent progress on combining geomorphological and geochronological data with ice sheet modelling, demonstrated using the last British–Irish Ice Sheet. *Journal of Quaternary Science*, 36, 946–960.

Ely, J.C., Clark, C.D., Small, D. & Hindmarsh, R.C.A. (2019) ATAT 1.1, the Automated Timing Accordance Tool for comparing ice-sheet model output with geochronological data. *Geoscientific Model Development*, 12, 933–953.

Ely, J.C., Clark, C.D., Spagnolo, M., Stokes, C.R., Greenwood, S.L., Hughes, A.L.C. et al. (2016) Do subglacial bedforms comprise a size and shape continuum? *Geomorphology*, 257, 108–119.

Evans, D.J.A., Clark, C.D. & Mitchell, W.A. (2005) The last British Ice Sheet: A review of the evidence utilised in the compilation of the Glacial Map of Britain. *Earth-Science Reviews*, 70, 253–312.

Evans, D.J.A., Harrison, S., Vieli, A. & Anderson, E. (2012) The glaciation of Dartmoor: the southernmost independent Pleistocene ice cap in the British Isles. *Quaternary Science Reviews*, 45, 31–53.

Evans, D.J.A., Roberts, D.H., Bateman, M.D., Clark, C.D., Medialdea, A., Callard, L. et al. (2021) Retreat dynamics of the eastern sector of the British–Irish Ice Sheet during the last glaciation. *Journal of Quaternary Science*, 36, 723–751.

Evans, D.J.A. & Thomson, S.A. (2010) Glacial sediments and landforms of Holderness, eastern England: a glacial depositional model for the North Sea Lobe of the British–Irish Ice Sheet. *Earth-Science Reviews*, 101, 147–189.

Everest, J. & Kubik, P. (2006) The deglaciation of eastern Scotland: cosmogenic 10Be evidence for a Lateglacial stillstand. *Journal of Quaternary Science*, 21, 95–104.

Feldmann, J., Albrecht, T., Khroulev, C., Pattyn, F. & Levermann, A. (2014) Resolution-dependent performance of grounding line motion in a shallow model compared with a full-Stokes model according to the MISMIP3d intercomparison. *Journal of Glaciology*, 60, 353–360.

Fisher, D.A., Reeh, N. & Langley, K. (1985) Objective reconstructions of the Late Wisconsinan Laurentide Ice Sheet and the significance of deformable beds. *Géographie physique et Quaternaire*, 39, 229–238.

Forsström, P.L., Sallasmaa, O., Greve, R. & Zwinger, T. (2003) Simulation of fast-flow features of the Fennoscandian ice sheet during the Last Glacial Maximum. *Annals of Glaciology*, 37, 383–389.

Gandy, N., Gregoire, L.J., Ely, J.C., Clark, C.D., Hodgson, D.M., Lee, V. et al. (2018) Marine ice sheet instability and ice shelf buttressing of the Minch Ice Stream, northwest Scotland. *The Cryosphere*, 12(11), 3635–3651. Available from https://doi.org/10.5194/tc-12-3635-2018

Gandy, N., Gregoire, L.J., Ely, J.C., Cornford, S.L., Clark, C.D. & Hodgson, D.M. (2019) Exploring the ingredients required to successfully model the placement, generation, and evolution of ice streams in the British-Irish Ice Sheet. *Quaternary Science Reviews*, 223, 105915.

Gandy, N., Gregoire, L.J., Ely, J.C., Cornford, S.L., Clark, C.D. & Hodgson, D.M. (2021) Collapse of the last Eurasian Ice Sheet in the North Sea modulated by combined processes of ice flow, surface melt, and marine ice sheet instabilities. *Journal of Geophysical Research: Earth Surface*, 126, 2020JF005755.

Geikie, J. 1894. The Great Ice Age. 3rd Edit.

Gemmell, A.M.D., Murray, A.S. & Connell, E.R. (2007) Devensian glacial events in Buchan (NE Scotland): A progress report on new OSL dates and their implications. *Quaternary Geochronology*, 2, 237–242.

Gladstone, R.M., Payne, A.J. & Cornford, S.L. (2010) Parameterising the grounding line in flow-line ice sheet models. *The Cryosphere*, 4, 605–619.

Gomez, N., Pollard, D. & Mitrovica, J.X. (2013) A 3-D coupled ice sheet–sea level model applied to Antarctica through the last 40 ky. *Earth and Planetary Science Letters*, 384, 88–99.

Gowan, E.J., Tregoning, P., Purcell, A., Lea, J., Fransner, O.J., Noormets, R. et al. (2016) ICESHEET 1.0: a program to produce paleo-ice sheet reconstructions with minimal assumptions. *Geoscientific Model Development*, 9, 1673–1682.

Gowan, E.J., Zhang, X., Khosravi, S., Rovere, A., Stocchi, P., Hughes, A.L.C. et al. (2021) A new global ice sheet reconstruction for the past 80 000 years. *Nature Communications*, 12, 1199.

Graham, A., Lonergan, L. & Stoker, M. (2007) Evidence for Late Pleistocene ice stream activity in the Witch Ground Basin, central North Sea, from 3D seismic reflection data. *Quaternary Science Reviews*, 26, 627–643.

Greenwood, S.L. & Clark, C.D. (2009) Reconstructing the last Irish Ice Sheet 1: changing flow geometries and ice flow dynamics deciphered from the glacial landform record. *Quaternary Science Reviews*, 28, 3085–3100.

Gregoire, L.J., Otto-Bliesner, B., Valdes, P.J. & Ivanovic, R. (2016) Abrupt Bølling warming and ice saddle collapse contributions to the Meltwater Pulse 1a rapid sea level rise. *Geophysical Research Letters*, 43, 9130–9137.

Gregoire, L.J., Payne, A.J. & Valdes, P.J. (2012) Deglacial rapid sea level rises caused by ice-sheet saddle collapses. *Nature*, 487, 219–222.

Gregoire, L.J., Valdes, P.J. & Payne, A.J. (2015) The relative contribution of orbital forcing and greenhouse gases to the North American deglaciation. *Geophysical Research Letters*, 42, 9970–9979.

Greve, R., Wyrwoll, K.H. & Eisenhauer, A. (1999) Deglaciation of the Northern Hemisphere at the onset of the Eemian and Holocene. *Annals of Glaciology*, 28, 1–8.

Hedges, R.E.M., Housley, R.A., Ramsey, C.B. & Van Klinken, G.J. (1994) Radiocarbon dates from the oxford ams system: Archaeometry datelist 18. *Archaeometry*, 36, 337–374.

Hiemstra, J.F., Shakesby, R.A. & Vieli, A. (2015) Late Quaternary glaciation in the Hebrides sector of the continental shelf: was St Kilda overrun by the British-Irish Ice Sheet? *Boreas*, 44, 178–196.

Hinck, S., Gowan, E.J., Zhang, X. & Lohmann, G. (2022) PISM-LakeCC: Implementing an adaptive proglacial lake boundary in an ice sheet model. *The Cryosphere*, 16, 941–965.

Hindmarsh, R.C.A. (2009) Consistent generation of ice-streams via thermo-viscous instabilities modulated by membrane stresses. *Geophysical Research Letters*, 36, 6.

Hjelstuen, B.O., Sejrup, H.P., Valvik, E. & Becker, L.W.M. (2018) Evidence of an ice-dammed lake outburst in the North Sea during the last deglaciation. *Marine Geology*, 402, 118–130.

Howe, J.A., Dove, D., Bradwell, T. & Gafeira, J. (2012) Submarine geomorphology and glacial history of the Sea of the Hebrides, UK. *Marine Geology*, 315-318, 64–76.

Hubbard, A., Bradwell, T., Golledge, N., Hall, A., Patton, H., Sugden, D. et al. (2009) Dynamic cycles, ice streams and their impact on the extent, chronology and deglaciation of the British–Irish ice sheet. *Quaternary Science Reviews*, 28, 758–776.

Hughes, A.L.C., Clark, C.D. & Jordan, C.J. (2014) Flow-pattern evolution of the last British Ice Sheet. *Quaternary Science Reviews*, 89, 148–168.

Hughes, A.L.C., Gyllencreutz, R., Lohne, Ø.S., Mangerud, J. & Svendsen, J.I. (2016) The last Eurasian ice sheets–a chronological database and time-slice reconstruction, DATED-1. *Boreas*, 45, 1–45.

Jacobi, R.M., Rose, J., MacLeod, A. & Higham, T.F.G. (2009) Revised radiocarbon ages on woolly rhinoceros (Coelodonta antiquitatis) from western central Scotland: significance for timing the extinction of woolly rhinoceros in Britain and the onset of the LGM in central Scotland. *Quaternary Science Reviews*, 28, 2551–2556.

Jardine, W.G., Dickson, J.H., Haughton, P.D.W., Harkness, D.D., Bowen, D.Q. & Sykes, G.A. (1988) A late Middle Devensian interstadial site at Sourlie, near Irvine, Strathclyde. *Scottish Journal of Geology*, 24, 288–295.

Ji, W., Robel, A., Tziperman, E. & Yang, J. (2021) Laurentide ice saddle mergers drive rapid sea level drops during glaciations. *Geophysical Research Letters*, 48, 2021GL094263.

Johnson, R.H., Tallis, J.H. & Wilson, P. (1990) The Seal Edge Coombes, North Derbyshire—a study of their erosional and depositional history. *Journal of Quaternary Science*, 5, 83–94.

Kirchner, N., Ahlkrona, J., Gowan, E.J., Lötstedt, P., Lea, J.M., Noormets, R. et al. (2016) Shallow ice approximation, second order shallow ice approximation, and full Stokes models: A discussion of their roles in palaeo-ice sheet modelling and development. *Quaternary Science Reviews*, 147, 136–147.

Kleman, J. & Glasser, N. (2007) The subglacial thermal organisation (STO) of ice sheets. *Quaternary Science Reviews*, 26, 585–597.

Kyrke-Smith, T.M., Katz, R.F. & Fowler, A.C. (2015) Subglacial hydrology as a control on emergence, scale, and spacing of ice streams. *Journal of Geophysical Research: Earth Surface*, 120, 1501–1514.

Lawson, T.J. (1984) Reindeer in the Scottish quaternary. *Quaternary Newsletter*, 42, 7.

Li, Y., Napieralski, J. & Harbor, J. (2008) A revised automated proximity and conformity analysis method to compare predicted and observed spatial boundaries of geologic phenomena. *Computers & Geosciences*, 34, 1806–1814. Available from: https://doi.org/10.1016/j.cageo.2008.01.003

Li, Y., Napieralski, J., Harbor, J. & Hubbard, A. (2007) Identifying patterns of correspondence between modeled flow directions and field evidence: an automated flow direction analysis. *Computers & Geosciences*, 33, 141–150.

Livingstone, S.J., Cofaigh, C.Ó. & Evans, D.J.A. (2010) A major ice drainage pathway of the last British–Irish Ice Sheet: the Tyne Gap, northern England. *Journal of Quaternary Science*, 25, 354–370.

Lockhart, E.A. 2020. *Glacial sculpting and post-glacial drowning of the Celtic Sea*. Bangor University (United Kingdom).

Lockhart, E.A., Scourse, J.D., Praeg, D., Van Landeghem, K.J.J., Mellett, C., Saher, M. et al. (2018) A stratigraphic investigation of the Celtic Sea megaridges based on seismic and core data from the Irish-UK sectors. *Quaternary Science Reviews*, 198, 156–170.

MacAyeal, D.R. (1993) Binge/purge oscillations of the Laurentide ice sheet as a cause of the North Atlantic's Heinrich events. *Paleoceanography*, 8, 775–784.

Margold, M., Stokes, C.R. & Clark, C.D. (2015) Ice streams in the Laurentide Ice Sheet: Identification, characteristics and comparison to modern ice sheets. *Earth-Science Reviews*, 143, 117–146.

Marshall, S.J. & Clarke, G.K.C. (1999) Ice sheet inception: subgrid hypsometric parameterization of mass balance in an ice sheet model. *Climate Dynamics*, 15, 533–550.

Martin, M.A., Winkelmann, R., Haseloff, M., Albrecht, T., Bueler, E., Khroulev, C. et al. (2011) The Potsdam parallel ice sheet model (PISM-PIK)–Part 2: dynamic equilibrium simulation of the Antarctic ice sheet. *The Cryosphere*, 5, 727–740.

Mas e Braga, M., Selwyn-Jones, R., Newall, J.C.H., Rogozhina, I., Andersen, J.L., Lifton, N.A. et al. (2021) Nunataks as barriers to ice flow: implications for palaeo ice sheet reconstructions. *The Cryosphere*, 15, 4929–4947.

Matsuoka, K., Hindmarsh, R.C.A., Moholdt, G., Bentley, M.J., Pritchard, H.D., Brown, J. et al. (2015) Antarctic ice rises and rumples: Their properties and significance for ice-sheet dynamics and evolution. *Earth-science reviews*, 150, 724–745.

McCabe, A.M. & Clark, P.U. (2003) Deglacial chronology from County Donegal, Ireland: implications for deglaciation of the British–Irish ice sheet. *Journal of the Geological Society*, 160, 847–855.

McCabe, A.M., Clark, P.U., Clark, J. & Dunlop, P. (2007) Radiocarbon constraints on readvances of the British–Irish Ice Sheet in the northern Irish Sea Basin during the last deglaciation. *Quaternary Science Reviews*, 26, 1204–1211.

McKay, M.D. (1992) Latin hypercube sampling as a tool in uncertainty analysis of computer models. In: *Proceedings of the 24th conference on Winter simulation*. pp. 557–564.

Merritt, J.W., Connell, E.R. & Hall, A.M. (2017) Middle to Late Devensian glaciation of north-east Scotland: implications for the north-eastern quadrant of the last British–Irish Ice Sheet. *Journal of Quaternary Science*, 32, 276–294.

Mitchell, W.A. (1994) Drumlins in ice sheet reconstructions, with reference to the western Pennines, northern England. *Sedimentary Geology*, 91, 313–331.

Murton, D. (2021) Hemingbrough Chronostratigraphy: Have BRITICE-CHRONO got it right? *Quaternary Newsletter*, 154, 1–7.

Napieralski, J., Li, Y. & Harbor, J. (2006) Comparing predicted and observed spatial boundaries of geologic phenomena: Automated Proximity and Conformity Analysis applied to ice sheet reconstructions. *Computers & Geosciences*, 32, 124–134. Available from: https://www.sciencedirect.com/science/article/pii/S0098300405001287

Niu, L., Lohmann, G., Hinck, S., Gowan, E.J. & Krebs-Kanzow, U. (2019) The sensitivity of Northern Hemisphere ice sheets to atmospheric forcing during the last glacial cycle using PMIP3 models. *Journal of Glaciology*, 65, 645–661.

Ó Cofaigh, C. & Dowdeswell JA. (2001) Laminated sediments in glacimarine environments: diagnostic criteria for their interpretation. *Quaternary Science Reviews*, 20, 1411–1436.

Ó Cofaigh, C., Callard, S.L., Roberts, D.H., Roberts, D.H., Chiverrell, R.C., Ballantyne, C.K. et al. (2021) Timing and pace of ice-sheet withdrawal across the marine–terrestrial transition west of Ireland during the last glaciation. *Journal of Quaternary Science*, 36, 805–832.

Ó Cofaigh, C. & Evans, D.J.A. (2007) Radiocarbon constraints on the age of the maximum advance of the British–Irish Ice Sheet in the Celtic Sea. *Quaternary Science Reviews*, 26, 1197–1203.

Ó Cofaigh, C., Telfer, M.W., Bailey, R.M. & Evans, D.J.A. (2012) Late Pleistocene chronostratigraphy and ice sheet limits, southern Ireland. *Quaternary Science Reviews*, 44, 160–179.

Ottesen, D., Stokes, C.R., Bøe, R., Rise, L., Longva, O., Thorsnes, T. et al. (2016) Landform assemblages and sedimentary processes along the Norwegian Channel Ice Stream. *Sedimentary Geology*, 338, 115–137.

Patton, H., Hubbard, A., Andreassen, K., Auriac, A., Whitehouse, P.L., Stroeven, A.P. et al. (2017) Deglaciation of the Eurasian ice sheet complex. *Quaternary Science Reviews*, 169, 148–172.

Patton, H., Hubbard, A., Andreassen, K., Winsborrow, M. & Stroeven, A.P. (2016) The build-up, configuration, and dynamical sensitivity of the Eurasian ice-sheet complex to Late Weichselian climatic and oceanic forcing. *Quaternary Science Reviews*, 153, 97–121.

Patton, H., Hubbard, A., Bradwell, T., Glasser, N.F., Hambrey, M.J. & Clark, C.D. (2013) Rapid marine deglaciation: asynchronous retreat

dynamics between the Irish Sea Ice Stream and terrestrial outlet glaciers. *Earth Surface Dynamics*, 1, 53–65.

Patton, H., Hubbard, A., Heyman, J., Alexandropoulou, N., Lasabuda, A.P.E., Stroeven, A.P. et al. (2022) The extreme yet transient nature of glacial erosion. *Nature Communications*, 13(1). Available from: https://doi.org/10.1038/s41467-022-35072-0

Peacock, J.D., Austin, W.E.N., Selby, I., Graham, D.K., Harland, R. & Wilkinson, I.P. (1992) Late Devensian and Flandrian palaeoenvironmental changes on the Scottish continental shelf west of the Outer Hebrides. *Journal of Quaternary Science*, 7, 145–161.

Peltier, W.R. (2004) Global glacial isostasy and the surface of the ice-age Earth: the ICE-5G (VM2) model and GRACE. *Annual Review of Earth and Planetary Sciences*, 32, 111–149.

Peters, J.L., Benetti, S., Dunlop, P. & Ó Cofaigh, C. (2015) Maximum extent and dynamic behaviour of the last British–Irish Ice Sheet west of Ireland. *Quaternary Science Reviews*, 128, 48–68.

Peters, J.L., Benetti, S., Dunlop, P., Ó Cofaigh, C., Moreton, S.G., Wheeler, A.J. et al. (2016) Sedimentology and chronology of the advance and retreat of the last British-Irish Ice Sheet on the continental shelf west of Ireland. *Quaternary Science Reviews*, 140, 101–124.

Petrini, M., Colleoni, F., Kirchner, N., Hughes, A.L.C., Camerlenghi, A., Rebesco, M. et al. (2020) Simulated last deglaciation of the Barents Sea Ice Sheet primarily driven by oceanic conditions. *Quaternary Science Reviews*, 238, 106314.

Phillips, W.M., Hall, A.M., Mottram, R., Fifield, L.K. & Sugden, D.E. (2006) Cosmogenic 10Be and 26Al exposure ages of tors and erratics, Cairngorm Mountains, Scotland: timescales for the development of a classic landscape of selective linear glacial erosion. *Geomorphology*, 73, 222–245.

Pollard, D. & DeConto, R.M. (2020) Continuous simulations over the last 40 million years with a coupled Antarctic ice sheet-sediment model. *Palaeogeography, Palaeoclimatology, Palaeoecology*, 537, 109374.

Praeg, D., McCarron, S., Dove, D., Ó Cofaigh, C., Scott, G., Monteys, X. et al. (2015) Ice sheet extension to the Celtic Sea shelf edge at the Last Glacial Maximum. *Quaternary Science Reviews*, 111, 107–112.

Reese, R., Albrecht, T., Mengel, M., Asay-Davis, X. & Winkelmann, R. (2018) Antarctic sub-shelf melt rates via PICO. *The Cryosphere*, 12, 1969–1985.

Robel, A.A. & Tziperman, E. (2016) The role of ice stream dynamics in deglaciation. *Journal of Geophysical Research: Earth Surface*, 121, 1540–1554.

Roberts, D.H., Evans, D.J.A., Callard, S.L., Clark, C.D., Bateman, M.D., Medialdea, A. et al. (2018) Ice marginal dynamics of the last British-Irish Ice Sheet in the southern North Sea: Ice limits, timing and the influence of the Dogger Bank. *Quaternary Science Reviews*, 198, 181–207.

Roberts, D.H., Grimoldi, E., Callard, L., Evans, D.J.A., Clark, C.D., Stewart, H.A. et al. (2019) The mixed-bed glacial landform imprint of the North Sea Lobe in the western North Sea. *Earth Surface Processes and Landforms*, 44, 1233–1258.

Robinson, M. & Ballantyne, C.K. (1979) Evidence for a glacial readvance pre-dating the Loch Lomond Advance in Wester Ross. *Scottish Journal of Geology*, 15, 271–277.

Rose, J. (1985) The Dimlington Stadial/Dimlington Chronozone: a proposal for naming the main glacial episode of the Late Devensian in Britain. *Boreas*, 14, 225–230.

Ross, H. 1996. *The last glaciation of Shetland*. University of St. Andrews (United Kingdom).

Schoof, C. (2006) Variational methods for glacier flow over plastic till. *Journal of Fluid Mechanics*, 555, 299–320.

Scourse, J., Saher, M., Van Landeghem, K.J.J., Lockhart, E., Purcell, C., Callard, L. et al. (2019) Advance and retreat of the marine-terminating Irish Sea Ice Stream into the Celtic Sea during the Last Glacial: Timing and maximum extent. *Marine Geology*, 412, 53–68.

Scourse, J.D., Austin, W.E.N., Bateman, R.M., Catt, J.A., Evans, C.D.R., Robinson, J.E. et al. (1990) Sedimentology and micropalaeontology of glacimarine sediments from the central and southwestern Celtic Sea. *Geological Society, London, Special Publications*, 53, 329–347.

Scourse, J.D., Chiverrell, R.C., Smedley, R.K., Small, D., Burke, M.J., Saher, M. et al. (2021) Maximum extent and readvance dynamics of the Irish sea ice stream and Irish Sea Glacier since the last glacial maximum. *Journal of Quaternary Science*, 36, 780–804.

Scourse, J.D. & Furze, M.F.A. (2001) A critical review of the glaciomarine model for Irish Sea deglaciation: evidence from southern Britain, the Celtic shelf and adjacent continental slope. *Journal of Quaternary Science*, 16, 419–434.

Scourse, J.D., Ward, S.L., Wainwright, A., Bradley, S.L. & Uehara, K. (2018) The role of megatides and relative sea level in controlling the deglaciation of the British–Irish and Fennoscandian ice sheets. *Journal of Quaternary Science*, 33, 139–149.

Seguinot, J., Ivy-Ochs, S., Jouvet, G., Huss, M., Funk, M. & Preusser, F. (2018) Modelling last glacial cycle ice dynamics in the Alps. *The Cryosphere*, 12(10), 3265–3285.

Sejrup, H.P., Clark, C.D. & Hjelstuen, B.O. (2016) Rapid ice sheet retreat triggered by ice stream debuttressing: evidence from the North Sea. *Geology*, 44, 355–358.

Sejrup, H.P., Haflidason, H., Aarseth, I., KING, E., FORSBERG, C.F., LONG, D. et al. (1994) Late Weichselian glaciation history of the northern North Sea. *Boreas*, 23, 1–13.

Simms, A.R., Best, L., Shennan, I., Bradley, S.L., Small, D., Bustamante, E. et al. (2022) Investigating the roles of relative sea-level change and glacio-isostatic adjustment on the retreat of a marine based ice stream in NW Scotland. *Quaternary Science Reviews*, 277, 107366.

Simpson, M.J.R., Milne, G.A., Huybrechts, P. & Long, A.J. (2009) Calibrating a glaciological model of the Greenland ice sheet from the Last Glacial Maximum to present-day using field observations of relative sea level and ice extent. *Quaternary Science Reviews*, 28, 1631–1657.

Small, D., Clark, C.D., Chiverrell, R.C., Smedley, R.K., Bateman, M.D., Duller, G.A.T. et al. (2017) Devising quality assurance procedures for assessment of legacy geochronological data relating to deglaciation of the last British-Irish Ice Sheet. *Earth-Science Reviews*, 164, 232–250.

Smedley, R.K., Scourse, J.D., Small, D., Hiemstra, J.F., Duller, G.A.T., Bateman, M.D. et al. (2017) New age constraints for the limit of the British–Irish Ice Sheet on the Isles of Scilly. *Journal of Quaternary Science*, 32, 48–62.

Smith, J.A., Callard, L., Bentley, M.J., Jamieson, S.S.R., Sánchez-Montes, M.L., Lane, T.P. et al. (2023) Holocene history of the 79°N ice shelf reconstructed from epishelf lake and uplifted glaciomarine sediments. *The Cryosphere*, 17, 1247–1270.

Stokes, C.R., Margold, M., Clark, C.D. & Tarasov, L. (2016) Ice stream activity scaled to ice sheet volume during Laurentide Ice Sheet deglaciation. *Nature*, 530, 322–326.

Stokes, C.R., Tarasov, L., Blomdin, R., Cronin, T.M., Fisher, T.G., Gyllencreutz, R. et al. (2015) On the reconstruction of palaeo-ice sheets: recent advances and future challenges. *Quaternary Science Reviews*, 125, 15–49.

Sutherland, D.G. & Walker, M.J.C. (1984) A late Devensian ice-free area and possible interglacial site on the Isle of Lewis, Scotland. *Nature*, 309, 701–703.

Tarasov, L., Dyke, A.S., Neal, R.M. & Peltier, W.R. (2012) A data-calibrated distribution of deglacial chronologies for the North American ice complex from glaciological modeling. *Earth and Planetary Science Letters*, 315-316, 30–40.

Tarasov, L. & Peltier, W.R. (2004) A geophysically constrained large ensemble analysis of the deglacial history of the North American ice-sheet complex. *Quaternary Science Reviews*, 23, 359–388.

Thomas, G., Chiverrell, R. & Huddart, D. (2004) Ice-marginal depositional responses to readvance episodes in the Late Devensian deglaciation of the Isle of Man. *Quaternary Science Reviews*, 23, 85–106.

Trotter, F.M., Hollingworth, S.E., Eastwood, T. & Rose, W.C.C. (1937) *Gosforth District*. Memoir of the Geological Survey of Great Britain, England and Wales, Sheet 37.

Tulaczyk, S., Kamb, W.B. & Engelhardt, H.F. (2000) Basal mechanics of Ice Stream B, west Antarctica: 2. Undrained plastic bed model. *Journal of Geophysical Research: Solid Earth*, 105, 483–494.

Van Landeghem, K.J.J. & Chiverrell, R.C. (2020) Bed erosion during fast ice streaming regulated the retreat dynamics of the Irish Sea Ice Stream. *Quaternary Science Reviews*, 245, 106526.

Van Pelt, W.J.J. & Oerlemans, J. (2012) Numerical simulations of cyclic behaviour in the Parallel Ice Sheet Model (PISM). *Journal of Glaciology*, 58, 347–360.

Von Weymarn, J. & Edwards, K.J. (1973) Interstadial site on the island of Lewis, Scotland. *Nature*, 246, 473–474.

Whittington, G. & Hall, A.M. (2002) The Tolsta Interstadial, Scotland: correlation with D–O cycles GI-8 to GI-5? *Quaternary Science Reviews*, 21, 901–915.

Williams, G.D., Brabham, P.J., Eaton, G.P. & Harris, C. (2001) Late Devensian glaciotectonic deformation at St Bees, Cumbria: a critical wedge model. *Journal of the Geological Society*, 158, 125–135.

Wilson, P., Dunlop, P., Millar, C. & Wilson, F.A. (2019) Age determination of glacially-transported boulders in Ireland and Scotland using Schmidt-hammer exposure-age dating (SHD) and terrestrial cosmogenic nuclide (TCN) exposure-age dating. *Quaternary Research*, 92, 570–582.

Winkelmann, R., Martin, M.A., Haseloff, M., Albrecht, T., Bueler, E., Khroulev, C. et al. (2011) The Potsdam parallel ice sheet model (PISM-PIK)–Part 1: Model description. *The Cryosphere*, 5, 715–726.

Winsborrow, M.C.M., Clark, C.D. & Stokes, C.R. (2010) What controls the location of ice streams? *Earth-Science Reviews*, 103, 45–59.

Ziemen, F.A., Kapsch, M.L., Klockmann, M. & Mikolajewicz, U. (2019) Heinrich events show two-stage climate response in transient glacial simulations. *Climate of the Past*, 15, 153–168.